JGR Atmospheres

RESEARCH ARTICLE
10.1029/2023JD040632

Methane Emissions From Seabed to Atmosphere in Polar Oceans Revealed by Direct Methane Flux Measurements

Evelyn Workman[1,2], Rebecca E. Fisher[2], James L. France[2,3], Katrin Linse[1], Mingxi Yang[4], Thomas Bell[4], Yuanxu Dong[4,5,6], and Anna E. Jones[1]

[1]British Antarctic Survey, Natural Environment Research Council, Cambridge, UK, [2]Centre of Climate, Oceans and Atmosphere (COCOA), Department of Earth Sciences, Royal Holloway University of London, Egham, UK, [3]Environmental Defense Fund, London, UK, [4]Plymouth Marine Laboratory, Plymouth, UK, [5]Centre for Ocean and Atmospheric Sciences, School of Environmental Sciences, University of East Anglia, Norwich, UK, [6]Now at Marine Biogeochemistry Research Division, GEOMAR Helmholtz Centre for Ocean Research Kiel, Kiel, Germany and Institute of Environmental Physics, Heidelberg University, Heidelberg, Germany

Key Points:

- Coastal regions of the Arctic Ocean and Southern Ocean are found to be sources of atmospheric methane
- The ocean releases elevated quantities of methane where seabed methane seeps have been observed in both the Arctic and Southern Oceans
- This study suggests a possible rise in methane release from oceanic areas with seabed seeps over last decades compared with a prior study

Supporting Information:

Supporting Information may be found in the online version of this article.

Correspondence to:

E. Workman,
eveman85@bas.ac.uk

Citation:

Workman, E., Fisher, R. E., France, J. L., Linse, K., Yang, M., Bell, T., et al. (2024). Methane emissions from seabed to atmosphere in polar oceans revealed by direct methane flux measurements. *Journal of Geophysical Research: Atmospheres*, *129*, e2023JD040632. https://doi.org/10.1029/2023JD040632

Received 20 DEC 2023
Accepted 14 JUL 2024

Author Contributions:

Conceptualization: Evelyn Workman, Rebecca E. Fisher, James L. France, Katrin Linse, Mingxi Yang, Thomas Bell, Anna E. Jones
Data curation: Evelyn Workman, Katrin Linse, Anna E. Jones
Formal analysis: Evelyn Workman, Rebecca E. Fisher, James L. France, Mingxi Yang, Thomas Bell, Anna E. Jones
Funding acquisition: Rebecca E. Fisher, James L. France, Katrin Linse, Mingxi Yang, Thomas Bell, Anna E. Jones
Investigation: Evelyn Workman, Mingxi Yang, Thomas Bell, Anna E. Jones
Methodology: Evelyn Workman, Rebecca E. Fisher, James L. France, Mingxi Yang, Thomas Bell, Anna E. Jones

Abstract

Sea-air methane flux was measured directly by the eddy-covariance method across approximately 60,000 km of Arctic and Antarctic cruises during a number of summers. The Arctic Ocean (north of 60°N, between 20°W and 50°E) and Southern Ocean (south of 50°S, between 70°W and 30°E) are found to be on-shelf sources of atmospheric methane with mean sea-air fluxes of 9.17 ± 2.91 (SEM (standard error of the mean)) μmol m^{-2} d^{-1} and 8.98 ± 0.91 μmol m^{-2} d^{-1}, respectively. Off-shelf, this region of the Arctic Ocean is found to be a source of methane (mean flux of 2.39 ± 0.68 μmol m^{-2} d^{-1}), while this region of the Southern Ocean is found to be a methane sink (mean flux of −0.77 ± 0.37 μmol m^{-2} d^{-1}). The highest fluxes observed are found around west Svalbard, South Georgia, and South Shetland Islands and Bransfield Strait; areas with evidence of the presence of methane flares emanating from the seabed. Hence, this study may provide evidence of direct emission of seabed methane to the atmosphere in both the Arctic and Antarctic. Comparing with previous studies, the results of this study may indicate an increase in sea-air flux of methane in areas with seafloor seepage over timescales of several decades. As climate change exacerbates rising water temperatures, continued monitoring of methane release from polar oceans into the future is crucial.

Plain Language Summary

The amount of methane released from oceans into the atmosphere is uncertain. Most oceanic methane is stored in the seabed and can escape into the water at seafloor seeps, but the extent to which it escapes into the atmosphere remains unclear. This study uses a relatively new method, eddy-covariance, to measure sea-air methane fluxes during Arctic and Antarctic cruises. This is the first time this technique has been applied to sea-air methane fluxes in both polar oceans. Our findings show that on-shelf regions of the Arctic and Southern Oceans release methane into the atmosphere, with average fluxes of 9.17 ± 2.91 μmol m^{-2} d^{-1} and 8.98 ± 0.91 μmol m^{-2} d^{-1}, respectively. We also identified areas with significant methane release in regions where methane has been found seeping into the water from the seabed. This study provides potential evidence that methane from seabed seeps may be directly emitted into the atmosphere in both the Arctic and Antarctic. Comparing with earlier studies, there is indication that the amount of methane released has increased over the last decades. As climate change drives increasing water temperatures, there is a potential for increased methane release from the seabed into the atmosphere, therefore on-going observations of methane release from polar oceans are necessary.

1. Introduction

Atmospheric methane (CH_4) is a potent greenhouse gas with natural and anthropogenic sources. CH_4 is important in terms of the Earth's radiative balance as it has a global warming potential between 80 and 83 times that of CO_2 over a 20-year period (Forster et al., 2021). Concentrations have been significantly increasing over the past few decades (Saunois et al., 2020), from about 700 ppb in pre-industrial times to ~1900 ppb in 2021 (Lan et al., 2023) which poses a problem for future climate change goals. The contribution that oceans have to the global CH_4 cycle is largely uncertain.

The dominant processes producing CH_4 in the ocean occur at the seafloor. CH_4 is produced in the sediments predominantly biogenically by microbial mediated CO_2 reduction in anoxic marine sediments (Formolo, 2010; Hinrichs & Boetius, 2002; Reeburgh, 1980; Whiticar, 1999), or by thermal breakdown of organic matter. Most

Project administration: Anna E. Jones
Resources: Evelyn Workman, Rebecca E. Fisher, James L. France, Mingxi Yang, Thomas Bell, Yuanxu Dong, Anna E. Jones
Supervision: Rebecca E. Fisher, James L. France, Katrin Linse, Mingxi Yang, Thomas Bell, Anna E. Jones
Visualization: Evelyn Workman
Writing – original draft: Evelyn Workman, Rebecca E. Fisher, James L. France, Katrin Linse, Anna E. Jones
Writing – review & editing: Evelyn Workman, Rebecca E. Fisher, James L. France, Katrin Linse, Mingxi Yang, Thomas Bell, Yuanxu Dong, Anna E. Jones

CH_4 produced in reduced sediments is consumed by anaerobic oxidation of methane (AOM) within the sediments (Barnes & Goldberg, 1976), and a smaller proportion can be consumed by aerobic methane oxidation in the presence of oxygen. Sedimentary CH_4 can also be trapped in hydrates. The CH_4 that is not consumed by AOM or aerobic methane oxidation within the marine sediments can be released into the water column through natural gas seeps or mud volcanoes (Judd et al., 2002), or from degrading hydrates (Skarke et al., 2014), in the form of bubbles (ebullition) or dissolved in water (Reeburgh, 2007). As bubbles of CH_4 rise through the water column, most of the CH_4 is dissolved in the surrounding water. Microbes in the water can convert the dissolved CH_4 into CO_2 via aerobic oxidation (Hanson & Hanson, 1996; Leonte et al., 2020; Murrell, 2010), or water with raised CH_4 concentrations can be diluted by mixing with surrounding waters. If the dissolved CH_4 is at the water surface it can be released into the atmosphere through diffusion (Joung et al., 2022). Water body overturning due to storms has also been correlated with CH_4 release, as storms can increase the interface between the sea surface and the atmosphere (Shakhova et al., 2014, 2015), and could increase mixing in the water column thus enhancing transport of CH_4 from sediments in shallow waters. The amount of CH_4 transported to the surface depends on seafloor depth and bubble characteristics (e.g., size, abundance and surface coating) (McGinnis et al., 2006; Rehder et al., 1998; Wang et al., 2016). Due to the activity in the water column (both biotic and abiotic), little CH_4 is actually able to travel to the surface and into to the atmosphere (Ruppel & Kessler, 2017), unless in the case of large volumes of methane released and/or sufficiently shallow seafloor. Gas bubble emissions from the seafloor can be detected using hydroacoustic equipment, and are referred to as "flares" due to their flame-like appearance on an echogram (Römer et al., 2014).

A large amount of CH_4 is stored at the seabed in sediments along continental margins of the Arctic Ocean (~100–9000 Gt C) (Biastoch et al., 2011; Hunter et al., 2013; Kretschmer et al., 2015; Kvenvolden, 1988). In the Arctic Ocean hydrates occur at shallower depths than in non-polar oceans, as they are stabilized at shallower depths by cold water temperatures (Hester & Brewer, 2009; Kvenvolden, 1993; Ruppel, 2011). Due to shallower GHSZ and rising ocean temperatures, gas hydrates in the Arctic Ocean are vulnerable to dissociation under future climate change scenarios (Biastoch et al., 2011; James et al., 2016; Marín-Moreno et al., 2013). The Southern Ocean is less well studied with respect to CH_4 than the Arctic Ocean. The presence of hydrates have been inferred on the South Shetland continental margin, the Ross Sea continental margin and the Wilkes Land continental margin (Giustiniani & Tinivella, 2021). Methane seeps have been observed in some coastal areas around Antarctica, including next to Seymour Island in the Weddell Sea (del Valle et al., 2017) and in the Ross Sea (Thurber et al., 2020), where bubbling has been seen as recently as 2023 (Seabrook et al., 2023). Human caused climate change has resulted in warming of the Southern Ocean (Fox-Kemper et al., 2021), notably, the bottom waters of the Southern Ocean (deeper than 2,000 m) have warmed faster than the global average.

It is thought that oceans act as a small net source of atmospheric CH_4, with recent estimates of ~1%–3% (Saunois et al., 2020) of the global methane budget. The strength of the oceanic source shifts when considering coastal oceans which dominate global ocean CH_4 emissions to the atmosphere (Bange et al., 1994; Borges et al., 2016; Weber et al., 2019), as these areas are shallower and there is higher riverine and estuarine water input, which can contain more CH_4 (Bange et al., 1994; Rehder et al., 1998; Upstill-Goddard et al., 2000). Freshwater systems are typically more enriched in CH_4 as the anaerobic conditions prevalent in freshwater sediments can create an optimal environment for methanogenic archaea to thrive (Bastviken et al., 2004; Borrel et al., 2011). Additionally, more CH_4 can be produced in freshwater systems due to the lower salinity conditions being more favorable for methanogens, compared with the higher salinity conditions found in oceans (Hartman et al., 2024). Freshwater systems typically have more dissolved organic carbon from terrestrial inputs, providing C substrates for methanogenic bacteria (Bertora et al., 2018). Methane-enriched freshwater from inland can enter coastal oceans via rivers. Furthermore, nutrient runoff from land can cause eutrophication of coastal waters leading to greater CH_4 production (Beaulieu et al., 2019). In polar regions alternative pathways can occur. Methanogenic archaea can produce CH_4 in subglacial sediments by anaerobic degradation of organic carbon (Boyd et al., 2010; Stibal et al., 2012). Subglacial meltwater has been found to be supersaturated with CH_4 on Greenland and Iceland (Burns et al., 2018; Christiansen & Jørgensen, 2018; Lamarche-Gagnon et al., 2019). This supersaturated meltwater can flow into the ocean via proglacial streams. A recent study has found that glacial retreat can lead to CH_4 release to the atmosphere, due to the formation of methane-rich groundwater springs in the forefields of the retreating glaciers (Kleber et al., 2023).

As a result of anthropogenic climate change, oceans are getting warmer (Fox-Kemper et al., 2021), and the IPCC AR6 report has stated with virtual certainty that the heat content of the global oceans will continue to increase over the 21st century (Fox-Kemper et al., 2021). Under future ocean warming, it is possible that significant oceanic CH_4 could be released, particularly on margins where gas hydrates are only just within the gas hydrate stability zone (GHSZ) (Joung et al., 2022), which may lead to a positive feedback loop in climate warming (Borges et al., 2016). Past warming events such as the Paleocene-Eocene Thermal Maximum have been hypothetically linked to methane release from dissociating gas hydrates (Dickens et al., 1995). Changes in terrestrial contributions could also occur with climate warming, such as the potential rise in freshwater runoff due to ice melting in polar regions, which could subsequently increase the CH_4 flux particularly in the high latitudes. Future warming may cause instability in CH_4 reservoirs beneath ice sheets due to marginal thinning of the ice sheet and glacial retreat, both of which could lead to increased CH_4 flux from meltwater in proglacial streams. Therefore, continuous monitoring of CH_4 sea-air fluxes is necessary to understand how anthropogenic climate change is currently impacting/will impact the oceanic contribution to the global CH_4 budget.

In this study, we quantify the amount of CH_4 released from regions of the Arctic Ocean (Greenland Sea, Barents Sea and Norwegian Sea) and Southern Ocean (Drake Passage, Scotia Sea, Weddell Sea, Bellingshausen Sea, and the South Shetland Islands and Bransfield Strait) by analyzing a sea-air CH_4 flux data set. Most previous studies calculate sea-air CH_4 fluxes in the Arctic and Southern Oceans using the bulk flux method, which calculates the flux due to diffusion across the sea-air interface. However, in this study, we analyze sea-air CH_4 fluxes calculated using the eddy-covariance (EC) technique, which is a more direct method to derive sea-air fluxes, as this method can detect direct emissions of methane to the atmosphere (by ebullition), in addition to diffusion. Sea-air fluxes measured by EC have been used as an independent reference for bulk air-sea CO_2 fluxes (Dong, Yang, Bakker, Liss, et al., 2021), but have not been used as widely for CH_4. EC is a relatively novel approach to measuring CH_4 fluxes from the polar oceans, to the best of our knowledge we are only aware of one other published result in the Arctic Ocean (Thornton et al., 2020), and none in the Southern Ocean. Therefore, this study provides unique new insights into CH_4 released from the ocean in the polar regions.

2. Methods

2.1. Eddy-Covariance Theory

Typically, sea-air CH_4 flux is estimated indirectly using the bulk flux equation (Liss, 1973),

$$F = k(C_w - HC_a), \tag{1}$$

where C_w is the dissolved CH_4 concentration in the water, H is the Henry's law constant (solubility), C_a is the atmospheric CH_4 concentration, and k is the gas transfer velocity, which is dependent on wind speed.

However, in this study a more direct method for measuring sea-air CH_4 flux is used, eddy-covariance (EC). The EC method measures and calculates vertical turbulent fluxes in the atmosphere using the equation,

$$F = \rho\overline{w'c'}, \tag{2}$$

where ρ is the mean mole density of dry air, w is the vertical wind velocity, and c is dry CH_4 mixing ratio in air. The prime denotes the fluctuations from the mean, and the overbar denotes temporal averaging. In this study w is measured by a sonic anemometer, and c is measured by a fast-response gas analyzer. The EC method can be preferable for measuring gas transfer as it is potentially more appropriate for measuring small-scale processes at the sea-air interface, it does not require water measurements, and it includes ebullition.

2.2. Instrumental Setup

CH_4 sea-air fluxes were measured onboard RRS *James Clark Ross (JCR)* during the period January 2019 to March 2021. Atmospheric CH_4 was measured with a Picarro G2311-f. This instrument is based on wavelength-scanned cavity ring-down spectroscopy (WS-CRDS) and measures CO_2, CH_4 and H_2O simultaneously at 10 Hz. Sea-air CH_4 fluxes were then calculated from fluctuations in atmospheric CH_4 measurements and wind speed measurements, as in Equation 2.

Table 1
Cruise, Date, Location and Distance Covered for Eight Cruises on RRS JCR That Measured Sea-Air EC CH_4 Fluxes

Cruise	Date period	Region	Approx. distance covered (km)
JR18004	06/01/2019–17/02/2019	Drake Passage, Scotia Sea, Weddell Sea.	9,500
JR18005	21/02/2019–15/04/2019	South Scotia Sea, South Scotia Ridge, South Sandwich Trench, northern Weddell Sea.	13,000
JR18006	30/06/2019–01/08/2019	Barents Sea, Arctic Ocean.	9,000
JR18007	05/08/2019–29/09/2019	Greenland Sea.	4,000
JR19001	15/11/2019–26/12/2019	Drake Passage, Scotia Sea, Weddell Sea.	5,000
JR19002	31/12/2019–09/03/2020	Scotia Sea, Bellingshausen Sea.	12,000
Logistics01	15/11/2020–30/11/2020	Trans-Atlantic.	8,000
Logistics02	02/12/2020–23/03/2021	Drake Passage, Scotia Sea, Weddell Sea, Bellingshausen Sea, Trans-Atlantic.	28,500

The instrumental setup on the *JCR* is described in detail in Dong, Yang, Bakker, Kitidis, and Bell (2021), however we outline the fundamentals here. The installed systems for CH_4 flux and data logging on the *JCR* operated autonomously. The EC system was located at the top of the foremast (approximately 20 m a.m.s.l). The EC system was comprised of a three-dimensional sonic anemometer (Metek Inc., Sonic-3 Scientific), a motion sensor (initially Systron Donner Motionpak II, which was replaced by a Life Performance-Research LPMS-RS232AL2 in April 2019), and a Picarro G2311-f greenhouse gas analyzer.

All instruments were operated at a sampling frequency of 10 Hz or higher, and the collected wind and motion data was logged using a Campbell Scientific, Inc. data logger, and greenhouse gas concentrations logged on a Picarro hard drive, both at a frequency of 10 Hz. Air was pulled in from the inlet at the mast through a 30 m tube (inner diameter 0.95 cm) by a dry vane pump with a flow rate of ≈40 L/min. The Picarro gas analyzer subsampled air through a particle filter (Swagelok 2 μ m) and a dryer (Nafion PD-200T-24M) which removed 80% of water vapor from the air and essentially all the water vapor fluctuations which ensured stability in humidity levels. The Picarro's internal calculations compensated for any remaining water vapor, providing a dry CH_4 mixing ratio for subsequent flux calculations. A "puff" of nitrogen is injected into the start of the inlet tube for 30 s every 6 hr to estimate time delay. The CH_4 mixing ratio data were filtered based on wind direction to remove data points when the air could be impacted by the ship stack.

2.3. Description of Cruises

The data used in this study (Workman et al., 2024) was taken onboard the *JCR* during six scientific cruises and two logistic cruises (Table 1). There are two cruises in the Arctic Ocean (JR18006 and JR18007) and five cruises in the Southern Ocean (JR18004, JR18005, JR19001, JR19002, and Logistics02). The remaining cruise (Logistics01) traversed the Atlantic Ocean from north to south. The last part of Logistics02 also traversed the Atlantic Ocean (south to north).

2.4. Data Processing

The data processing method is detailed in Dong, Yang, Bakker, Kitidis, and Bell (2021) (e.g., see Section 2.2 and flowchart in Fig. 2 of Dong, Yang, Bakker, Kitidis, and Bell (2021)), but is briefly described here in the context of CH_4 fluxes rather than CO_2 fluxes. The raw high-frequency wind and CH_4 data are processed to calculate fluxes in 20 min intervals. Related statistics are used for quality control. Linear detrending is employed to identify turbulent fluctuations (w' and c'). Ship motion is corrected by applying a complementary filtering method using Euler angles which eliminates apparent winds caused by ship movements. The motion-corrected winds are decorrelated against ship motion and double-rotated to account for the wind streamline over the ship. The resulting vertical wind velocity (w) is used to calculate flux (Equation 2). The processed wind data is used to compute variables such as friction velocity and sensible heat flux. CH_4 data is despiked, decorrelated against analyzer cell pressure and temperature, and decorrelated against factors related to ship motion. A lag (of a few seconds) between CH_4 and wind data is addressed using a puff system or the maximum covariance method. The inlet tube, particle filter, and dryer introduce attenuation in CH_4 flux signals, which is compensated for in the calculations. Horizontal CH_4 fluxes and other statistics are computed for quality control. Finally, the computed

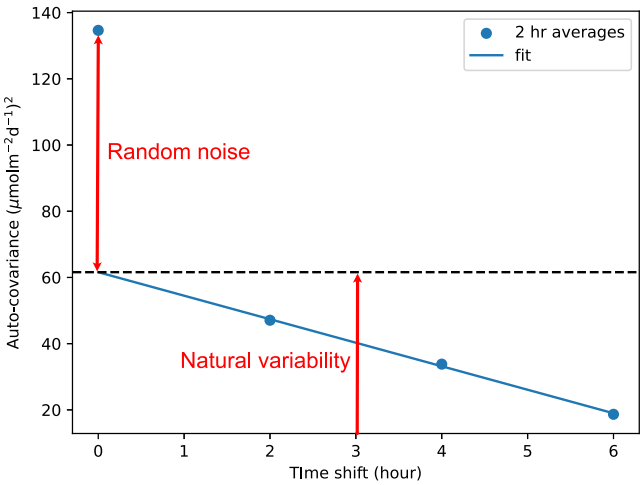

Figure 1. Auto-covariance of 2-hourly flux data set (cruise JR19001) at various time shifts (points) and a line of best fit to the natural variability auto-covariance function extrapolated back to a zero time shift. Each time shift is one time step forward in the 2 hr averaged flux time series.

fluxes undergo filtering to exclude non-ideal ship maneuvers or violations of the EC technique requirements. 20 min intervals that pass the QA/QC (Quality Assurance/Quality Control) are further averaged to 2 hr to reduce noise. QA/QC filters used are given in Text S1 in Supporting Information S1. The eddy-covariance data used in this study are open access and published by the UK Polar Data Centre (PDC) (Workman et al., 2024).

2.5. Emission Uncertainty

The uncertainty in EC CH_4 flux is derived in analogous fashion to EC CO_2 flux, as described in (Dong, Yang, Bakker, Kitidis, & Bell, 2021; Yang, Bell, et al., 2016; Yang, Prytherch, et al., 2016). The vast majority of the uncertainty is from random noise, most of which is due to natural variability in CH_4 mixing ratio. We do not consider oceanic instability as highly unstable conditions are rare for the Southern and Arctic Oceans. Even during occasions when the sea surface is much warmer than the air above, wind speeds are usually sufficiently high such that the atmosphere is not far from neutral.

2.6. Calculating Limit of Detection

CH_4 sea-air fluxes are generally small so it is necessary to find a way to distinguish between a genuine flux signal and noise. Therefore, we calculate the limit of detection (LoD) for our flux data set. LoD is the lowest signal that can be reliably detected with a given analytical method. Typically, LoDs are defined as being 3 times higher than the signal from the random noise. The observed variance in CH_4 flux comprises of random noise and natural variability. The autocovariance of a time series is related to random noise and natural variability by,

$$\sigma^2(t \to 0) = \sigma^2_{rand} + \sigma^2_{nat}, \tag{3}$$

where, $\sigma^2(t \to 0)$ is the autocovariance at zero time shift, σ_{rand} is the standard deviation of random noise, and σ_{nat} is the standard deviation of natural variability (Dong, Yang, Bakker, Kitidis, & Bell, 2021). The autocovariance measures the covariance between a time series and a lagged version of itself. Autocovariance is calculated using the equation detailed in Text S2 in Supporting Information S1.

To calculate the random noise we can plot the autocovariance of the flux time series at varying time shifts (Figure 1). Random noise only correlates with itself, however natural variability tends to retain some correlation even with some offset in time. Therefore, at non-zero time shifts the observed variance only comprises of natural variability. Extrapolating the autocovariance to time shift zero based on the linear trend of the autocovariance at non-zero time shifts, we can infer the natural variability at time shift zero (Figure 1). The random noise is then calculated by taking the difference between the autocovariance at time shift zero and the autocovariance extrapolated to time shift zero (i.e., natural variability at time shift zero), as in Equation 3.

As the LoD is typically 3 times greater than the signal from random noise, we can calculate LoD by,

$$\text{LoD} = 3 * \sigma_{rand}. \tag{4}$$

2.7. Sea Depth Data

We obtain the sea depth data for each two-hour averaged data point using the General Bathymetric Chart of the Ocean (GEBCO) data set (GEBCO Compilation Group, 2023) for data points north of 50°S and the International Bathymetric Chart of the Southern Ocean (IBCSO) data set (Dorschel et al., 2022) for data points south of 50°S.

2.8. Echosounder Data

CH_4 flares can be detected in the water column using echosounders. The *JCR* is equipped with two single-beam echosounders, Simrad EK60 and EK80. There are four tranducer frequencies; 38 kHz, 70 kHz, 120 and 200 kHz. The EK data collected by the *JCR* echosounders can be replayed to identify any flares using Kongsberg Simrad

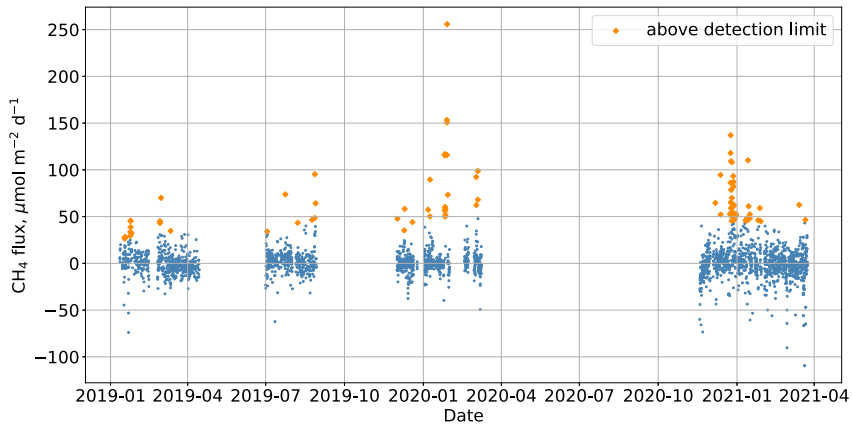

Figure 2. Two hour averaged sea-air CH_4 flux data set (Workman et al., 2024) taken onboard RRS *JCR* during cruises described in Table 1. The orange diamonds represent the fluxes above the calculated instrumental limit of detection, in the positive direction only.

EK80 software (Kongsberg, 2023). The single-beam echosounder is not operational at all times; there is only echosounder data corresponding to cruises JR19001 and JR19002. Therefore, of the cruises with CH_4 sea-air flux data (Table 1), we can only check for flare presence during cruises JR19001 and JR19002. During JR19001 the EK60 was operational at all four frequencies (data was not collected by EK80 during cruise). The EK60 was calibrated on 09/12/2019 in Stromness Harbor. The pulse length used was 1.024 ms for all frequencies. During JR19002 the EK80 was operational at three frequencies (38, 70 and 120 kHz), while EK60 data were not collected. EK80 was calibrated in Port Lockroy on 22/01/2020. The 38 and 120 kHz ran with 1 ms pulse length and the 70 kHz ran with 8 ms or 4 ms pulse length most of the time. The pulse type was continuous waveform (CW) for 38 kHz, CW and frequency modulated (FM) for 70 and 120 kHz.

CH_4 flares can also be identified in areas of interest (i.e., areas where this study identified elevated sea-air CH_4 fluxes) using echosounder data from previous *JCR* cruises and RRS *Sir David Attenborough (SDA)* cruises. *JCR* cruises which have corresponding EK data include Southern Ocean cruises from 2014 to 2018 (JR307, JR308, JR298, JR16002, JR16003, JR17002, JR17003a (all of which have EK60 data) and JR18003 (which has EK80 data)). A flare was only identified during cruise JR17002 in Deception Island caldera (see Section 3.5). The EK60 operated at frequencies 38, 70, 120, and 200 kHz during cruise JR17002 with pulse length 1.024 ms and was calibrated on 07/01/2018 in Stromness Harbor.

EK80 data taken on *SDA* during the polar science trial cruise SD025 in February/March 2023 was also investigated. *SDA* is equipped with a six frequency Simrad EK80 scientific echosounder operating at frequencies 18, 38, 70, 120, 200, and 333 kHz. During SD025 the EK80 was calibrated in the Weddell Sea on 10/03/2023. A pulse length of 1.024 ms was used for each frequency during the cruise and pulse type was CW. SDA has multibeam echosounder ME70 which is more appropriate for measuring seafloor seeps than a single beam echosounder as multibeam echosounders allow a greater area of the seafloor to be observed. However, there is no multibeam echosounder data for SD025 as the ME70 was not operational during the cruise.

In this study, the EK data is only used to identify, qualitatively, whether flares are present in areas of interest. In order to detect less obvious signals, a more thorough approach to analyzing EK data would be necessary (i.e., post-processing the data). Further analysis to reveal more subtle signals is planned for a follow-up study.

3. Results

3.1. Sea-Air Methane Fluxes

The LoDs for sea-air methane fluxes for the six science cruises and two logistic cruises are calculated (Table S1 in Supporting Information S1) for each cruise separately due to potential inconsistencies with the running of the Picarro between cruises. Additionally, the calculated standard deviation of the flux increases for later cruises (i.e., Logistics01 and Logistics02) compared to earlier cruises, signaling the instrument getting noisier over time. Therefore, it is more appropriate to calculate LoD for each cruise, rather than over the entire data set. In general,

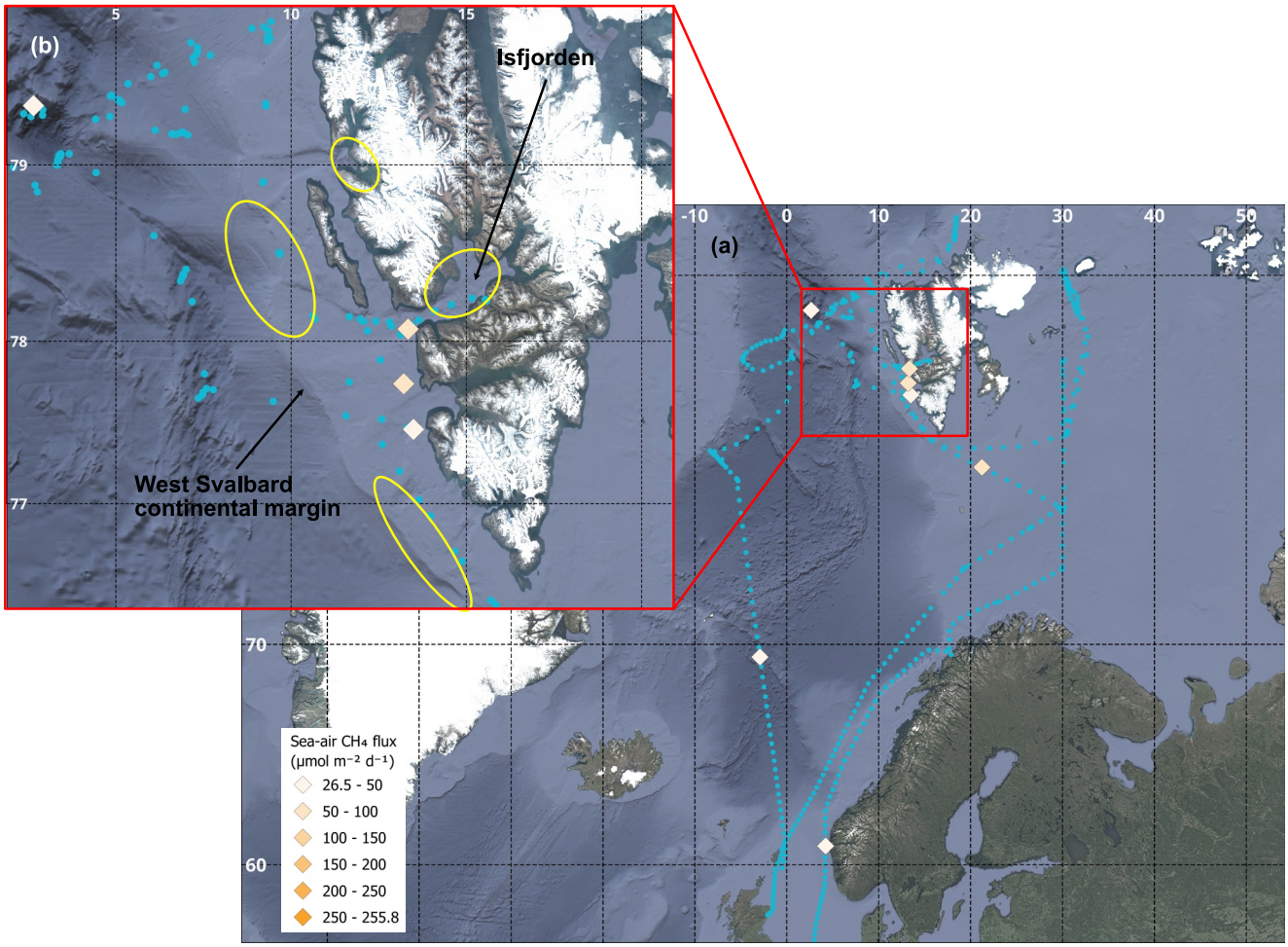

Figure 3. (a) Map showing each 2 hourly averaged sea-air CH_4 flux measurement (blue dots) and sea-air CH_4 fluxes which sit above the limit of detection (orange/white diamonds), during cruises JR18006 and JR18007 in the Arctic Ocean. The color of the diamond corresponds to the flux value, as seen on the scale. (b) Map zoomed into Western Svalbard showing areas where flares have been identified in previous studies (yellow circles) (Betlem et al., 2021; Bohrmann et al., 2015; Ferré et al., 2020; Mau et al., 2017; Roy et al., 2019; Sahling et al., 2014).

most data points are below the LoD (Figure 2). The LoD is lower for some cruises, that is, JR18004 and JR19001, due to the data being clustered together and less noisy. Random error accounts for the majority of the flux uncertainty (Dong, Yang, Bakker, Kitidis, & Bell, 2021).

3.2. Flux-Sea Depth Relationship

Higher sea-air CH_4 fluxes are expected in coastal regions with shallower waters (Weber et al., 2019). Here we test this hypothesis by dividing the data set into four regimes: near-shore (0–50 m), outer shelf (50–200 m), continental slope (200–2,000 m) and open ocean (2,000 m), following the method of Weber et al. (2019). The near-shore, outer shelf and continental slope act as a source of atmospheric CH_4 with mean fluxes of 13.65 ± 1.35 μmol m^{-2} d^{-1}, 7.16 ± 1.24 μmol m^{-2} d^{-1} and 4.23 ± 0.49 μmol m^{-2} d^{-1}, respectively, while we find the open ocean acts as a sink of atmospheric CH_4 with a mean fluxes of -1.34 ± 0.32 μmol m^{-2} d^{-1}. The errors quoted here and throughout are standard error of the mean. The data shows a clear trend; increasing distance from landmass decreases the magnitude of the CH_4 source.

3.3. Arctic Ocean (Greenland Sea, Norwegian Sea and Barents Sea)

In the Arctic Ocean, the study area constitutes of the region north of 60°N and between the longitudinal bounds 20°W and 50°E (Figure 3). This area is made up of regions of the Greenland Sea, Norwegian Sea and Barents Sea.

Table 2
Mean On-Shelf, Mean Off-Shelf and the Range of Sea-Air CH_4 Fluxes Found in This Study

Region	On-shelf mean (μmol m^{-2} d^{-1})	Off-shelf mean (μmol m^{-2} d^{-1})	Range (μmol m^{-2} d^{-1})
Arctic Ocean (north of 60°N, between 20°W and 50°E)	9.17 ± 2.91	2.39 ± 0.68	−62.3 to 95.3
Greenland Sea	2.95 ± 1.70	−0.13 ± 0.95	−31.6 to 46.6
Norwegian Sea	4.87 ± 3.22	3.28 ± 0.93	−24.2 to 34.0
Barents Sea	13.74 ± 5.25	1.15 ± 1.23	−62.3 to 73.8
West Svalbard and Isfjorden	12.96 ± 8.39	22.81 ± 5.60	−13.7 to 95.3
Southern Ocean (south of 50°S, between 70°W and 30°E)	8.98 ± 0.91	−0.77 ± 0.37	−90.33 to 255.77
Weddell Sea	1.64 ± 1.55	−0.54 ± 0.61	−56.02 to 52.43
Scotia Sea	8.26 ± 1.58	−0.25 ± 0.59	−60.60 to 98.80
Drake Passage	NA	−3.6 ± 1.93	−25.60 to 38.63
Bellinghausen Sea	11.51 ± 1.42	−2.50 ± 3.01	−34.58 to 137.04
South Shetland Islands and Bransfield Strait	34.13 ± 7.45	4.54 ± 2.07	−43.64 to 255.77
South Georgia	7.90 ± 1.60	1.17 ± 5.55	−44.68 to 98.80

Note. The errors quoted are standard error of the mean (SEM).

We obtained CH_4 flux data from two cruises: JR18006 and JR18007 (Table 1). 2-hour averaged sea-air CH_4 fluxes in this region of the Arctic vary between −62.3 and 95.3 μmol m^{-2} d^{-1} (Table 2).

We find a mean on-shelf sea-air flux and a mean off-shelf sea-air flux for the Arctic Ocean. We divide the data set up into these two categories as different processes are governing the CH_4 release resulting in shallower, on-shelf waters being a greater source of atmospheric CH_4 than deeper, off-shelf waters. In the context of the Arctic Ocean, the term "on-shelf" refers to areas with a depth of less than 200 m, assuming that it is the same as the average upper limit of ocean shelf depth globally (Emery, 1969). The on-shelf mean is 9.17 ± 2.91 μmol m^{-2} d^{-1}, while the off-shelf mean is 2.39 ± 0.68 μmol m^{-2} d^{-1} in boreal summertime. On-shelf and off-shelf means for the Greenland Sea, Norwegian Sea and Barents Sea are calculated and given in Table 2.

In order to calculate the total CH_4 release from each sea, we calculate a mean flux for each sea. We derive a scaled mean flux for each sea by adjusting the ratio of on-shelf to off-shelf data points in the flux data set to match the on-shelf to off-shelf ratio of the study area, using data from the GEBCO data set (GEBCO Compilation Group, 2023). The scaled mean is calculated by multiplying the on-shelf and off-shelf means by the percentage of the sea that is on-shelf and the percentage of the sea that is off-shelf, respectively, and adding them together. This adjustment is necessary to obtain a flux that is more representative of each sea because, as Table 2 shows, on-shelf regions are a greater source of atmospheric CH_4, hence associated with more positive fluxes. The scaled mean for the Greenland Sea, Norwegian Sea and Barents Sea is calculated to be 0.98 ± 0.87, 3.51 ± 0.92 and 6.35 ± 2.28 μmol m^{-2} d^{-1}, respectively. Using these scaled mean fluxes, we calculate the amount of CH_4 released from the Greenland Sea, Norwegian Sea and Barents Sea to be 0.6 ± 0.5 Gg, 2.5 ± 0.6 Gg and 4.5 ± 1.6 Gg per summer month, respectively.

There is a cluster of three fluxes above the limit of detection (LoD) west of Svalbard near Isfjorden (Figure 3). The mean on-shelf and off-shelf fluxes around the area of west Svalbard and Isfjorden (defined within the latitudinal range 76.25°N and 79.75°N and longitudinal range 11°E and 17°E) are 12.96 ± 8.39 μmol m^{-2} d^{-1} and 22.81 ± 5.60 μmol m^{-2} d^{-1}, respectively.

3.4. Southern Ocean (Weddell Sea, Scotia Sea, Drake Passage, Bellinghausen Sea, and South Shetland Islands and Bransfield Strait)

In the Southern Ocean, the study area constitutes of the region south of 50°S and between the longitudinal bounds of 70°W and 30°E (Figure 4). The study area comprises of regions of the Weddell Sea, Scotia Sea, Drake Passage, Bellinghausen Sea, and South Shetland Islands and Bransfield Strait. We obtained CH_4 flux data in this region from the cruises JR18004, JR18005, JR19001, JR19002, and Logistics02 (Table 1). The 2-hr averaged sea-air CH_4 fluxes in this region of the Southern Ocean vary between −90.33 and 255.77 μmol m^{-2} d^{-1} (Table 2).

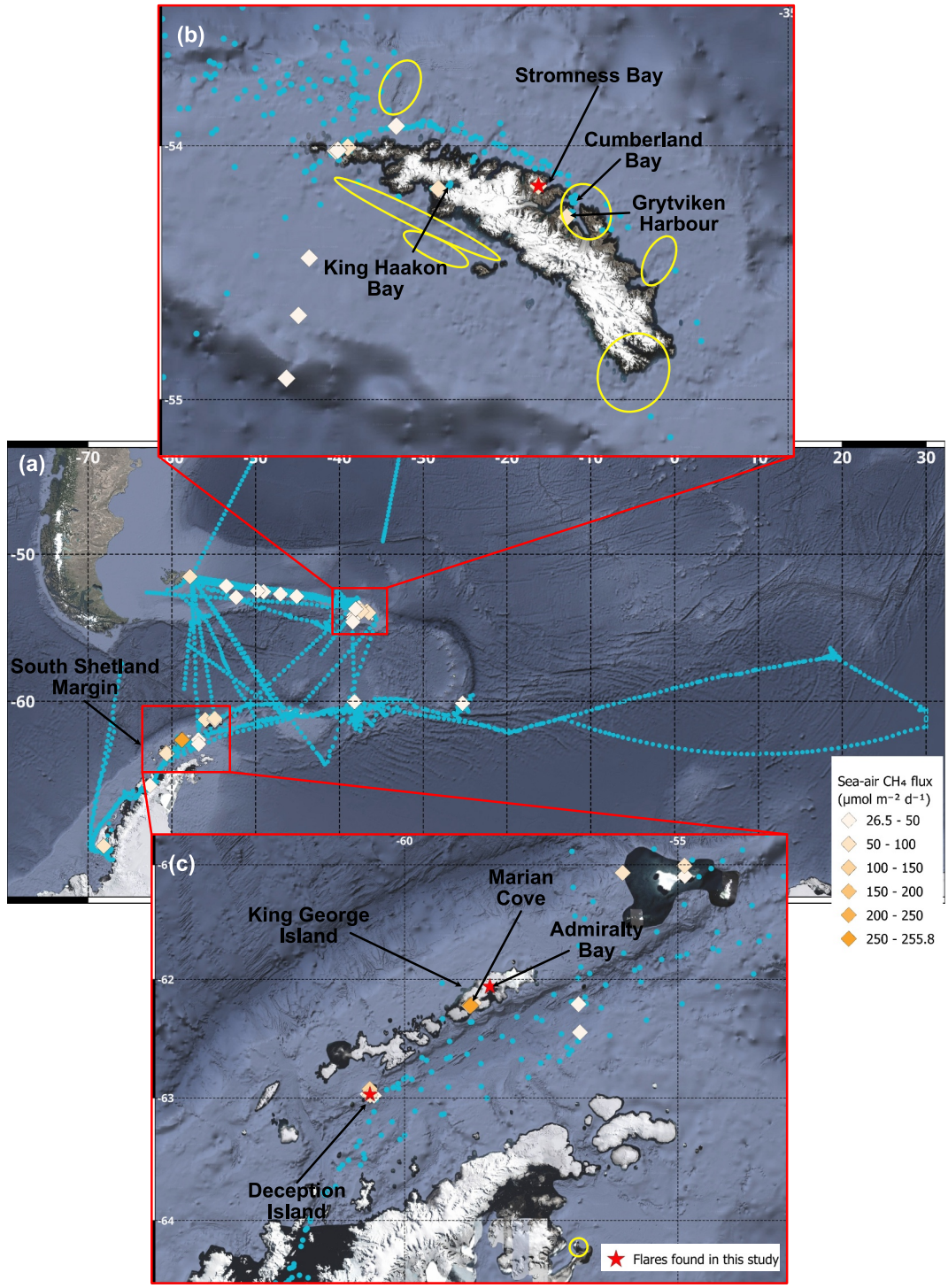

Figure 4. (a) Map showing each 2 hourly averaged sea-air CH_4 flux (blue dots) measurement and sea-air CH_4 fluxes which sit above the limit of detection (orange/white diamonds), during cruises JR18004, JR18005, JR19001, JR19002, and Logistics02 in the Southern Ocean. The color of the diamond corresponds to the flux value, as seen on the scale. Map zoomed into: (b) South Georgia, and (c) South Shetland Islands and Bransfield Strait. Red stars in (b) and (c) indicate flares identified in this study using EK60/EK80 data from RRS *JCR* and RRS *SDA* cruises, and areas where flares have been identified in previous studies (yellow circles) (Römer et al., 2014; Bohrmann et al., 2017; del Valle et al., 2017).

As with the CH_4 fluxes in the Arctic Ocean, we calculate a mean on-shelf flux and a mean off-shelf flux in the Southern Ocean. In the Southern Ocean, on-shelf is defined as shallower than 500 m (Heywood et al., 2014). The continental shelf in the Southern Ocean is deeper than other continental shelves due to factors such as ice sheet loading and erosion from past glaciations (Colleoni et al., 2018). The on-shelf mean flux is 8.98 ± 0.91 μmol m^{-2} d^{-1}, while the off-shelf mean is -0.77 ± 0.37 μmol m^{-2} d^{-1}. We divided the study area into individual areas (Weddell Sea, Scotia Sea, Drake Passage, Bellinghausen Sea, and South Shetland Islands and Bransfield Strait) and the on-shelf and off-shelf means are calculated (Table 2). Drake Passage did not have any flux data points which corresponded to depths shallower than 500 m, so therefore we could not compute an on-shelf mean.

We calculate and an on-shelf/off-shelf scaled mean flux for each of the areas (Weddell Sea, Scotia Sea, Drake Passage, Bellinghausen Sea, and South Shetland Islands and Bransfield Strait) using the same method as for the Arctic Ocean (Section 3.3). Using the scaled flux values, we calculate the amount of CH_4 released from Weddell Sea, Scotia Sea, Drake Passage, Bellinghausen Sea, and South Shetland Islands and Bransfield Strait during austral summer to be approximately -0.4 ± 1.9 Gg, 0.1 ± 0.6 Gg, -2.6 ± 3.4 Gg, 0.5 ± 1.2 Gg, and 0.5 ± 0.2 Gg per month, respectively. Negative values indicates that the region takes up atmospheric CH_4.

There are clusters of elevated fluxes (above LoD) around South Georgia Island and around the South Shetland Islands and Bransfield Strait (SS and BS) (Figure 4). South Georgia and the surrounding shelf, defined as between latitudinal range of 53.75°S and 55°S and longitudinal range of 35.5°W and 38.5°W, has an on-shelf and off-shelf mean CH_4 flux of 7.90 ± 1.60 and 1.17 ± 5.55 μmol m^{-2} d^{-1}, respectively. There are six different periods when the *JCR* was in the South Georgia area (Figure S2 in Supporting Information S1) with three of these periods having fluxes above LoD. In this study, SS and BS is defined as between the latitudinal range of 61°S and 64°S and the longitudinal range of 54°W to 63°W. The on-shelf and off-shelf mean CH_4 sea-air flux around SS and BS is 34.13 ± 7.45 and 4.54 ± 2.07 μmol m^{-2} d^{-1}, respectively. There are five different periods when the *JCR* is around the SS and BS (Figure S2 in Supporting Information S1) with three periods having fluxes above LoD.

3.5. Echosounder Data

Three potential seabed seepage events were identified in this study using EK60 and EK80 single beam echosounder data with the method described in Section 2.8. A flare was detected in the caldera of Deception Island using EK60 data collected on JCR cruise JR17002 on 20/01/2018 at 12:49:30 at coordinates (62.9719°S, 60.6328°W) (Figure 5b). A flare was detected in Stromness Bay using EK60 data collected on *JCR* crusie JR19001 on 10/12/2019 at 08:06:21 at coordinates (54.1589 S, 36.6917 W) (Figure 5a). Single bubbles rising from the seafloor were detected in Admiralty Bay, King George Island using EK80 data collected on *SDA* cruise SD025 on 25/02/2023 between 17:30:17 and 20:20:00 at coordinates (62.0609°S, 58.4384°W), while the ship was stationary (Figure 5c). Figure 5c depicts single rising bubbles as the SDA is stationary, and therefore does not show the characteristic flare as seen in Figures 5a and 5b.

4. Discussion

4.1. Flux-Sea Depth Relationship

More positive sea-air CH_4 fluxes are expected over shallower waters, and less positive fluxes over deeper, open ocean waters (Bange et al., 1994; Weber et al., 2019). The results of this study match this hypothesis, as we find near-shore (0–50 m), outer shelf (50–200 m), continental slope (200–2,000 m) regions act as a CH_4 source to the atmosphere with a mean sea-air CH_4 fluxes of 13.65 ± 1.35 μmol m^{-2} d^{-1}, 7.16 ± 1.24 μmol m^{-2} d^{-1} and 4.23 ± 0.49 μmol m^{-2} d^{-1}, respectively. These results show that the strength of the source decreases as we shift toward deeper waters. The open ocean (>2,000 m) acts as a CH_4 sink with a mean sea-air CH_4 flux of -1.34 ± 0.32 μmol m^{-2} d^{-1}.

The results of this study could indicate that seabed processes, including seafloor seepage, and terrestrial (including glacial) runoff are the dominant mechanisms producing the CH_4 that reaches the atmosphere. Shallower areas often coincide with coastal regions, where CH_4-enriched freshwater from land sources could be the primary contributor to atmospheric CH_4, given that freshwater environments generally exhibit higher CH_4 production compared to seawater environments (Saunois et al., 2020). Several factors contribute to the elevated concentration of CH_4 in freshwater including the higher organic content of freshwater, the reduced sulfate

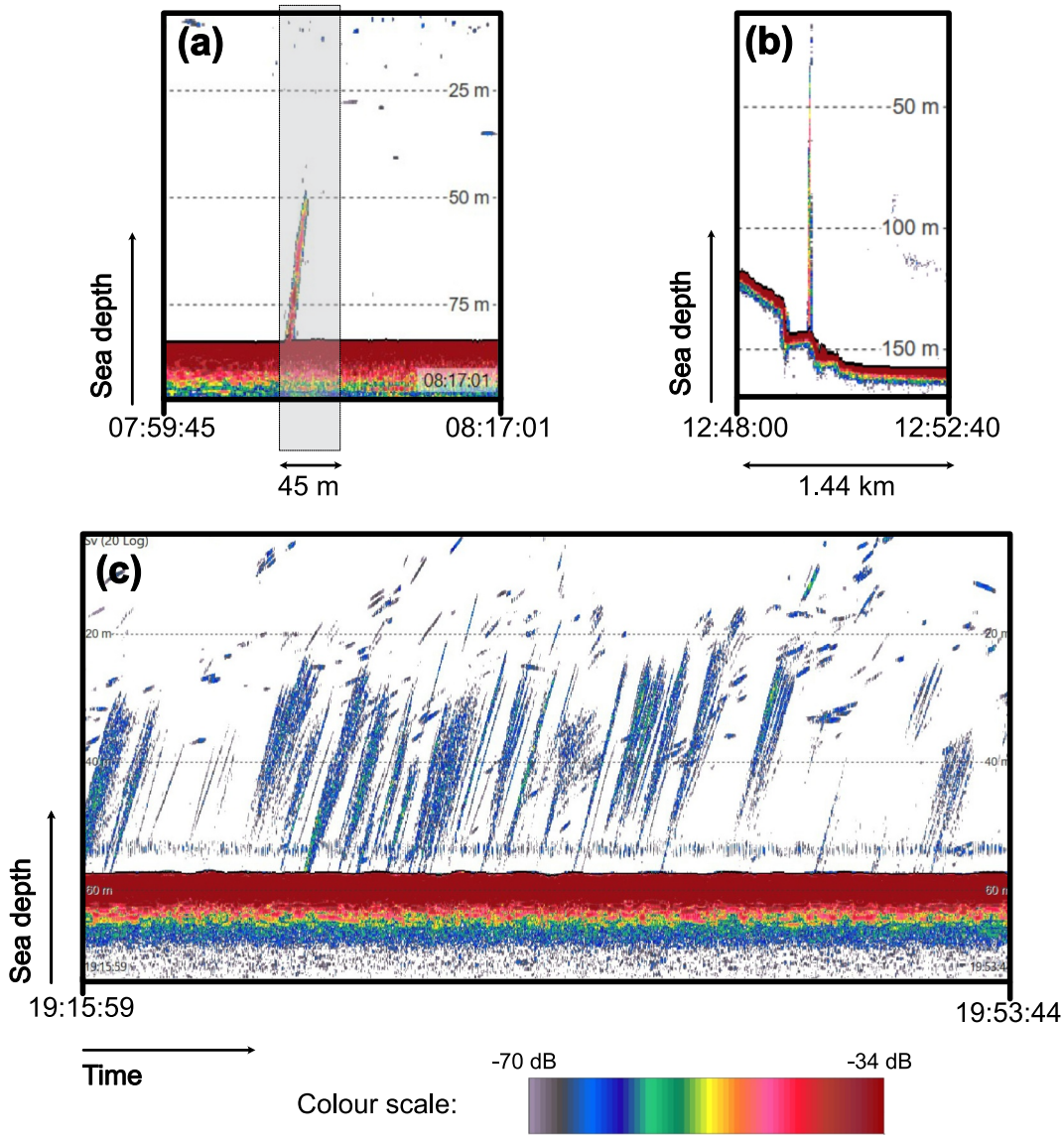

Figure 5. Echograms indicating possible seabed seepage events imaged at 38 kHz frequency with (a) EK60 echosounder in Cumberland Bay, South Georgia (54.1589°S, 36.6929°W) on 10/12/2019 at 08:06:21 on RRS *JCR* cruise JR19001 (data used can be found in Fielding (2024a)), (b) EK60 echosounder in Deception Island (62.9719°S, 60.6328°W) on 20/01/2018 at 12:49:30 on RRS *JCR* cruise JR17002 (data used can be found in Fielding and Manno (2024)), and (c) EK80 echosounder in Admiralty Bay, King George Island (62.0609°S, 58.4384°W) on 25/02/2023, single streams of bubble are seen rising from the seabed continuously between 17:30:17 and 20:20:00 on RRS *Sir David Attenborough* cruise SD025 (data used can be found in Fielding (2024b)). The *x*-axis represents time. The thick red line along the bottom of the echograms represents the seafloor. The *y*-axis is sea-depth. The distance along the seabed is indicated for when the ship is moving; (a) the ship is moving between 08:05:41 and 08:09:13 (indicated by gray box) with an average speed of 0.4 knots, and so distance moved is ∼45 m, (b) The ship is moving at average speed 10 knots and so moves a distance of ∼1.44 km, (c) the ship is stationary throughout time of echogram and so distance moved is 0 m. The colors represent the intensity of echoes returned to the echosounder, with the intensity quantified in decibels (dB) (between −70 dB and −34 dB). If the echo is stronger, the color will be more toward the red end of the scale, while weaker echoes will have a color toward the gray end. The EK80 data was replayed retrospectively on Simrad EK80 software (Kongsberg, 2023). The echograms are screen grabbed from this software.

concentration in freshwater sediments, which limits the presence of anaerobic methanotrophic archaea (ANME) responsible for CH_4 oxidation, and the anaerobic conditions prevalent in freshwater sediments, creating an optimal environment for methanogenic archaea to thrive (Rehder et al., 1998; Scranton & McShane, 1991). Subglacial runoff could be a source of CH_4 in polar coastal regions, as has been found in the Arctic (Christiansen

Table 3
Arctic Ocean Sea-Air CH_4 Fluxes From This Study and Previous Studies

Region	Flux (μmol m^{-2} d^{-1})	Year of measurement	Month(s)	Study
Bering Sea	0.2 ± 0.4	2015	July	Fenwick et al. (2017)
Eastern Chukchi Sea	1.9 ± 1.4	2015	July	Fenwick et al. (2017)
Canada Basin	1.3 ± 1.1	2015	September, October	Fenwick et al. (2017)
Canadian Arctic Archipelago	1.2 ± 1.1	2015	July	Fenwick et al. (2017)
North American Arctic Ocean	1.3 (−0.4–4.9)	2015	July–October	Fenwick et al. (2017)
Northern Labrador Sea and Baffin Bay	0.04 ± 0.03	2021	July, August	Vogt et al. (2023)
Davis Strait	1.6	2011	October	Punshon et al. (2014)
Greenland Sea	0.98 ± 0.87[a]	2019	July, August	This study
Norwegian Sea	3.51 ± 0.92[a]	2019	July, August	This study
Barents Sea	6.35 ± 2.28[a]	2019	July	This study
North of 60°N, between 20°W and 50°E (on-shelf)	9.17 ± 2.91[b]	2019	July and August	This study
North of 60°N, between 20°W and 50°E (off-shelf)	2.39 ± 0.68[b]	2019	July and August	This study
Laptev Sea	186.4	2014	July, August	Thornton et al. (2016)
Laptev Sea	285.5[b]	2014	July	Thornton et al. (2020)
East Siberian Sea	7, 17[c]	2003, 2004	September	Shakhova and Semiletov (2007)
East Siberian Sea	236.9	2014	July, August	Thornton et al. (2016)
East Siberian Sea	108.5[b]	2014	August	Thornton et al. (2020)
Chukchi Sea	8.7[b]	2014	August	Thornton et al. (2020)
Isfjorden and, West Svalbard	17.00 ± 5.46[a]	2019	July, August	This study
Svalbard	9 (Max)[d], (−0.36–0.072)[e]	2014	June, July	Pisso et al. (2016)
North Svalbard	92.8 ± 6.3 (Max)[f]	2014–2016	All	Platt et al. (2018)
West Svalbard	(8.64–13.68)[g]	2014	June–August	Myhre et al. (2016)
West Svalbard	(0.47–6.44)	2012, 2015	August, September	Mau et al. (2017)
NStorfjorden polynya	26, 104[h]	2003	March	Damm et al. (2007)

Note. Values are average, except for maximum values which are indicated by (Max) and ranges which are indicated in brackets. The table is divided up into western Arctic Ocean, eastern Arctic Ocean and Svalbard. [a]Measured using eddy-covariance method. Scaled on-shelf/off-shelf mean calculated using the method described in Section 3.3. [b]Measured using eddy-covariance method. [c]Area weighted mean flux. [d]Calculated using FLEXPART and stability model. [e]Budget calculation (Karion et al., 2013) using aircraft data in an area of known CH_4 seeps. [f]Calculated by normalizing the change in mixing ratio to the change in mean footprint sensitivity. [g]Range of maximum fluxes possible constrained by atmospheric observations. Calculated using three independent atmospheric models. [h]Values are calculated for wind speeds of 5 and 10 m/s, respectively.

& Jørgensen, 2018; Lamarche-Gagnon et al., 2019) and around the Antarctic Peninsula (Brusselman et al., 2024). The anaerobic conditions found beneath glaciers provide the optimal conditions for CH_4 production, resulting in outflow waters which are supersaturated in CH_4.

4.2. Arctic Ocean

The on-shelf and off-shelf regions of the Arctic Ocean investigated here (north of 60°N and between the longitudinal bounds 20°W and 50°E) are both found to be a summertime source of CH_4, with a mean sea-air CH_4 flux of 9.17 ± 2.91 μmol m^{-2} d^{-1} and 2.39 ± 0.68 μmol m^{-2} d^{-1}, respectively, in July and August 2019. On-shelf areas are found to be a greater source of CH_4 than off-shelf areas in general across the various regions of the Arctic Ocean investigated, apart from western Svalbard and Isfjorden (Table 2).

Previously reported sea-air CH_4 fluxes within the Arctic Ocean, as summarized in Table 3, exhibit significant heterogeneity across various geographical regions. This variability highlights the inherent non-uniform nature of the Arctic Ocean. Previous studies have, in general, found the western Arctic Ocean to be a very small/negligible source of CH_4. Vogt et al. (2023) reports a mean value of 0.039 ± 0.031 μmol m^{-2} d^{-1} for the northern Labrador Sea and Baffin Bay in July 2021. Fenwick et al. (2017) report a mean value of 1.3 μmol m^{-2} d^{-1} over the North

American Arctic Ocean in July, September, and October 2015. Punshon et al. (2014) find a flux of 1.6 μmol m^{-2} d^{-1} in the Davis Strait in 2011. In contrast, the eastern Arctic Ocean has been found to be a greater source of atmospheric CH_4 (10–100 times greater than other regions). For example, Thornton et al. (2016, 2020) find fluxes over the Laptev Sea of 186.4 μmol m^{-2} d^{-1} and 285.5 μmol m^{-2} d^{-1}, respectively. The Eastern Siberian Sea was found to have a flux of 108.5 μmol m^{-2} d^{-1} by Thornton et al. (2020), and Shakhova and Semiletov (2007) have found fluxes within the range 45–95 μmol m^{-2} d^{-1} in this region. The eastern Arctic Ocean has been found to be a greater source of atmospheric CH_4 than other regions of the Arctic Ocean due to the presence of submarine permafrost on the East Siberian shelf, which is not present on other shelf locations in the Arctic (Angelopoulos et al., 2020). Additionally, the water over the East Siberian shelf is relatively shallow compared to the rest of the Arctic shelf, which could lead to more seabed produced CH_4 reaching the atmosphere. Overall, the studies reviewed here generally find the Arctic Ocean to be a source of CH_4 across all regions. In this study, we find fluxes within the same order of magnitude as previous studies in similar areas (western Arctic Ocean).

We calculate the on-shelf and off-shelf mean fluxes separately as we assume these areas are distinct in terms of sea-air CH_4 fluxes. However, in Table 3, the fluxes quoted for Greenland Sea, Barents Sea, Norwegian Sea and Western Svalbard and Isfjorden in this study are on-shelf/off-shelf scaled means calculated using the method highlighted in Section 3.3. This is done so that we can compare the sea-air fluxes found in this study with those found in other study across similar areas, as previous studies do not differentiate between on-shelf and off-shelf.

Most previous studies calculate sea-air CH_4 flux using the bulk flux method, however in this study fluxes are measured in a more direct way, using eddy-covariance (EC) (Equation 2). Thornton et al. (2020), which investigates the eastern Arctic Ocean, is the only other Arctic Ocean study which measured fluxes using the EC method. Thornton et al. (2020) uses a Los Gatos Research (LGR) Fast Greenhouse Gas Analyzer (FGGA) to measure atmospheric CH_4 mixing ratios, while this study uses a Picarro G2311-f. Yang, Prytherch, et al. (2016) compared the performance of Picarro G2311-f and LGR FGGA for measuring CH_4 sea-air fluxes in a coastal area found that the Picarro G2311-f showed significantly lower noise levels than the LGR FGGA, indicating that the method we use in this study results in lower limits of detection.

We find that the Barents Sea is associated with the greatest sea-air CH_4 flux, followed by the Norwegian Sea and then the Greenland Sea. The higher flux over the Barents Sea could be explained using similar arguments which explain the greater flux found over the eastern Arctic Ocean in previous studies; the Barents Sea is shallower (~230 m) than the Norwegian (~2,000 m) or Greenland (~1,450 m) Seas, and there is some submarine permafrost present in the eastern Barents Sea (Angelopoulos et al., 2020). However, we only have flux data points from the west Barents Sea, so therefore, we may not expect to see a subsea permafrost CH_4 signal in our data set, as there is likely little subsea permafrost here (Angelopoulos et al., 2020).

Our findings indicate that combined the Greenland Sea, Barents Sea, and Norwegian Sea emit approximately 7.5 ± 1.8 Gg per month of CH_4 into the atmosphere during boreal summertime. In scaling up fluxes to calculate emissions we assume that the areas surveyed by the *JCR* in each sea are representative of that entire sea. By simplifying the analysis by applying an on-shelf/off-shelf scaling procedure to the mean flux, we assume that on-shelf/off-shelf processes are the dominant mechanisms governing CH_4 release. 7.5 ± 1.8 Gg per month of CH_4 accounts for ~0.01% of the global methane budget (Saunois et al., 2020) if we scale up to 1 year. Note that it is expected that the amount of CH_4 released is seasonally dependent, mainly due to the seasonal variability of sea-ice extent in the Arctic. The presence of more sea-ice may inhibit the sea-air exchange process completely (James et al., 2016). While we recognize that there is a small amount of sea-ice coverage (primarily in the northern Greenland Sea) in the summer, we do not consider the impact of sea-ice as it is beyond the scope of this study. Therefore, we assume that scaling up the amount of CH_4 released to compare with global yearly emissions gives the upper limit of yearly emissions from this area.

4.2.1. Isfjorden and West Svalbard

There is a cluster of fluxes above LoD west of Svalbard near Isfjorden (Figure 3b) in August during cruise JR18007. This area was found to be a larger source of atmospheric CH_4 compared to the whole study region. Several previous studies have used different methods to try and quantify the sea-air CH_4 fluxes around Svalbard, and there are a wide range of results, with some values being comparable to other regions of the western Arctic Ocean, and others being one or two orders of magnitude greater (Table 3). The mean on-shelf/off-shelf scaled flux

and the range in flux around west Svalbard and Isfjorden found in this study is within the same order of magnitude as previously recorded in the literature. The maximum sea-air flux in the literature is observed in Storfjorden polynya, south Svalbard, where Damm et al. (2007) calculated a maximum flux of 104 μmol m^{-2} d^{-1}. The authors attribute this high flux to CH_4 release from the seafloor during resuspension of sediments and propose a bacterial source of the CH_4 produced near the sediment surface. Platt et al. (2018) also finds a high sea-air CH_4 flux off the north coast of Svalbard. It is hypothesized that the source of this CH_4 is oceanic and originates at the seabed as CH_4 seeps have been found in the area (Geissler et al., 2016).

CH_4 seepage from the seafloor off the west coast of Svalbard (west Svalbard continental margin) has been extensively reported on as numerous studies have found gas flares in the water column (Dølven et al., 2022; Graves et al., 2015; Knies et al., 2004; Mau et al., 2017; Rajan et al., 2012; Sahling et al., 2014; Steinle et al., 2015; Veloso et al., 2019; Westbrook et al., 2009). It has been found that dissociation of gas hydrates at the West Svalbard continental margin play a role in the CH_4 seepage from the seafloor due to warming bottom waters in the area (Berndt et al., 2014; Westbrook et al., 2009). Additionally, Betlem et al. (2021) identify gas flares in Isfjorden, which they conclude could indicate an active petroleum system. However, only a few studies investigate how much CH_4 released from the seabed off the coast of Svalbard penetrates the sea-air barrier and enters the atmosphere. Myhre et al. (2016) find that CH_4 released from the seabed around Svalbard has limited impact on the atmospheric CH_4 levels in summer. Fisher et al. (2011) also comes to the same conclusion, finding that seeps have limited atmospheric impact during the summer.

Identifying the origin of the CH_4 associated with the elevated fluxes found in this study is difficult. The sea-air CH_4 fluxes above LoD off the west coast of Svalbard could be attributed to CH_4 originating from seabed seeps, as there is an abundance of evidence of CH_4 seeping from the seabed into the water column around this area. However, the elevated fluxes do not lie directly above the locations of known flares but are located east of the West Svalbard continental margin, closer to the coast (Figure 3). The West Spitsbergen Current (WSC) runs poleward just west of Svalbard, which suggests that the potential CH_4 saturated waters above the flares of the continental margin would be transported north rather than east. Hence, while the elevated CH_4 fluxes observed off the coast of Svalbard may not conclusively point to a seabed origin, it is impossible to determine this from the measurements we have. The elevated fluxes during this period could be attributed to elevated CH_4 concentrations in the water from CH_4-enriched freshwater outflow from the land (Damm et al., 2007). This hypothesis is supported by lower surface water salinity compared to the previous period in the same area (in July 2019 during JR18006). Potential sources of CH_4-enriched freshwater from Svalbard include streams, rivers, glaciers, and lakes (Damm et al., 2005; Hodson et al., 2020; Kleber et al., 2023). Additionally, it's noteworthy that during the periods of higher fluxes, the prevailing winds appear to be originating more from the landward direction. This suggests the possibility of terrestrial origins for freshwater in the upper waters. To establish the exact source of CH_4 contributing to these elevated fluxes, a more comprehensive study would be need to be carried out in this area which simultaneously measured EC sea-air CH_4 fluxes, dissolved CH_4 concentration in water and presence of flares measured using acoustics.

4.3. Southern Ocean

We find the study area of the Southern Ocean (south of 50°S and between 70°W and 30°E) to be an on-shelf source and off-shelf sink of CH_4 in austral summer. The on-shelf sea-air mean CH_4 flux in the Southern Ocean is the same as the on-shelf flux in the Arctic Ocean, within error. This could indicate that similar on-shelf processes are governing CH_4 release in the Southern and Arctic Oceans. These processes could include seabed seepage (e.g., South Georgia and South Shetland Islands) or freshwater and subglacial run off. We find that off-shelf Southern Ocean is a small sink of CH_4, with a negative sea-air CH_4 flux, which is contrasting to the off-shelf source found in the Arctic Ocean. Several previous studies have found that strong upwelling in the Southern Ocean brings deeper, CH_4 depleted water to the surface, making the surface waters undersaturated in CH_4 and therefore an atmospheric CH_4 sink (Heeschen et al., 2004; Weber et al., 2019). Previous studies have found heterogeneity across different areas of the Southern Ocean. Some areas are very small sources (positive fluxes) of CH_4, while others are very small sinks (negative fluxes) (Table 4). In general, open ocean areas of the Southern Ocean have been found to be sinks of CH_4 by previous studies, while areas that have been found to be sources are either coastal or exhibit high speed winds.

Table 4
Southern Ocean Sea-Air CH_4 Fluxes From This Study and Previous Studies

Region	Flux (μmol m^{-2} d^{-1})	Year of measurement	Month(s)	Study
Ross Sea	−0.44	2020	January	Ye et al. (2023)
Lat: 54°S–65°S; Lon: 160°W	2.3 ± 1.3	2001	December	Yoshida et al. (2011)
Lat: 54°S–65°S; Lon: 160°W	1.6 ± 1.0	2002	January	Yoshida et al. (2011)
Lat: 54°S–65°S; Lon: 160°W	2.1 ± 1.0	2002	February	Yoshida et al. (2011)
Bellinghausen Sea	2.09 ± 2.08[a]	2019, 2020, 2021	December–February	This study
Drake Passage	−0.35	1986, 1987	December–March	Tilbrook and Karl (1994)
Drake Passage	−3.60 ± 1.93[a]	2019, 2020, 2021	December–February	This study
SS and BS	0.69	1986, 1987	December–March	Tilbrook and Karl (1994)
SS and BS	18.85 ± 3.76[a]	2019, 2020, 2021	December–February	This study
Scotia Sea	0.17 ± 0.57[a]	2019, 2020, 2021	December–April	This study
Weddell Sea	−0.47	1998	March–May	Heeschen et al. (2004)
Weddell Sea	−0.29 ± 0.58[a]	2019, 2020, 2021	December–April	This study
Cumberland Bay, South Georgia	0.018	2013	March/April	Geprägs et al. (2016)
South Georgia	7.34 ± 1.54[a]	2019, 2020, 2021	December–March	This study
South of 50°N, between 70°W and 30°E (on-shelf)	8.98 ± 0.91	2019, 2020, 2021	December–April	This study
South of 50°N, between 70°W and 30°E (off-shelf)	−0.77 ± 0.37	2019, 2020, 2021	December–April	This study
Lat: 54°S–65°S; Lon: 140°E	0.8 ± 0.6	2001	December	Yoshida et al. (2011)
Lat: 54°S–65°S; Lon: 140°E	1.3 ± 0.7	2002	January	Yoshida et al. (2011)
Lat: 54°S–65°S; Lon: 140°E	2.0 ± 1.1	2002	February	Yoshida et al. (2011)
Entire Southern Ocean (south of −50°S)	0.09	2012	December	Bui et al. (2018)
Entire Southern Ocean (south of −50°S)	0.14	2013	January	Bui et al. (2018)
Entire Southern Ocean (south of −50°S)	0.06	2013	February	Bui et al. (2018)

Note. The table is ordered by region (west to east) and estimates of entire Southern Ocean are at the end. SS and BS = South Shetland Islands and Bransfield Strait.
[a]Measured using eddy-covariance method. Scaled on-shelf/off-shelf mean calculated using the method described in Section 3.4.

The results of this study indicate that the Weddell Sea, Scotia Sea, and Bellinghausen Sea are an on-shelf source of atmospheric CH_4, while off-shelf these seas are, within error, neither sink nor source of atmospheric CH_4. The Weddell Sea has been found to be a sink by Heeschen et al. (2004) and the authors state that the distribution of CH_4 in the Weddell Sea is controlled mainly by mixing between surface water and deeper waters, which is more depleted in CH_4. There are no previous studies which investigate CH_4 in the Bellinghausen or Scotia Seas, but the same upwelling mechanism could be at play as in the Weddell Sea. We find the Drake Passage to be an off-shelf sink of CH_4, which agrees with the findings of Tilbrook and Karl (1994). They find undersaturation in the surface waters which they attribute to entrainment of warm deep water, which is more depleted in CH_4, to the surface. In this study, we find that in the Southern Ocean only areas with known seabed seeps (South Georgia and South Shetland Islands and Bransfield Strait) are both on-shelf and off-shelf sources of CH_4.

The cumulative CH_4 uptake across the Weddell Sea, Bellinghausen Sea, Scotia Sea, Drake Passage, and South Shetland Islands and Bransfield Strait is calculated to be 1.9 ± 1.7 Gg per month. While this represents a noteworthy uptake of CH_4, its significance in the context of the global CH_4 budget is minimal. When extrapolated over a year, this uptake amounts to approximately 0.003% of the total annual global CH_4 emissions (Saunois et al., 2020). However, the exchange of CH_4 across the sea-air interface exhibits seasonal variability, for example, sea-ice may inhibit exchange of CH_4 (James et al., 2016). In the summer months, when sea-ice extent is reduced, the uptake of CH_4 is likely to be greater. Therefore scaling up the summertime exchange of CH_4 to the whole year likely over estimates the amount of CH_4 taken up, meaning that the ∼0.003% estimation of the global methane budget is likely an overestimate.

4.3.1. South Georgia

There is a cluster of fluxes above LoD around the island of South Georgia (Figure 4b). The on-shelf and off-shelf waters around South Georgia are sources of CH_4 to the atmosphere. There are 16 fluxes above LoD around South Georgia and they are highlighted in Table S2 in the Supporting Information S1.

Numerous seabed CH_4 seeps have been identified around the island (Bohrmann et al., 2017; Römer et al., 2014). Sea-air CH_4 flux measurements provide a novel data set for this area and can help us to understand if CH_4 produced in the seabed around South Georgia reaches the atmosphere. Seabed produced CH_4 could be the source of the elevated sea air flux (above LoD) in Stromness Bay. We identified a CH_4 flare during JR19001 on 10/12/2019 at 08:06:21 at coordinates (54.1589°S, 36.6917°W), using EK60 data (Figure 5a) in Stromness Bay close to when the elevated flux was observed. This provides evidence that the increased sea-air flux could be attributed to seabed produced CH_4. The two elevated fluxes in Grytviken harbor, Cumberland Bay could be due to seabed produced CH_4 as numerous flares have been previously identified in Cumberland Bay, including in areas close to Grytviken harbor, in studies by Römer et al. (2014) and Bohrmann et al. (2017). The water depth here is also very shallow, which means it is possible that seabed released CH_4 could make it to the surface, either dissolved in the water or through ebullition. However, Geprägs et al. (2016) find a sea-air CH_4 flux of 0.018 μmol m^{-2} d^{-1} in Cumberland Bay (using the bulk flux method), indicating that almost no CH_4 reaches the atmosphere despite seeing evidence of seabed flares in Cumberland Bay, and raised CH_4 concentrations throughout the water column above flares.

An additional potential origin of CH_4 in the surface waters surrounding South Georgia arises from proglacial discharge, which can be supersaturated with CH_4 (Andrews, 2019). This phenomena offers an explanation for the elevated fluxes in King Haakon Bay, as there is a coinciding decrease in salinity. We cannot rule out seabed seepage as a possible source of CH_4 here, however, no flares have been identified in this bay in previous studies, and there is no *JCR* or *SDA* EK60/EK80 data from this bay, limiting our ability to conduct a comprehensive analysis of potential seabed seepage in this area.

4.3.2. South Shetland Islands and Bransfield Strait

There is a cluster of sea-air CH_4 fluxes above LoD around SS and BS, NW of the Antarctic Peninsula (Figure 4c). We find that the on-shelf and off-shelf waters around SS and BS are a source of CH_4 to the atmosphere. There are 24 flux observations above LoD around SS and BS and they are highlighted in Table S3 in the Supporting Information S1.

SS and BS is the area with the highest on-shelf flux of CH_4 in this study. Tilbrook and Karl (1994) found that this area was a small source of CH_4 in 1986/1987 with a flux of 0.69 μmol m^{-2} d^{-1}. Our results could imply a change in the amount of CH_4 released from this area over the 30 years between the two sets of measurements. While we note the these two studies use different observational techniques, the on-shelf and off-shelf fluxes we calculate here are one to two orders of magnitude greater than that found by Tilbrook and Karl (1994) in the late 1980s (Tables 2 and 4), which would unlikely be accounted for by different observational approaches. This suggests that the discrepancies between these two studies is due to a physical phenomena. However, CH_4 fluxes/seabed seeps can occur episodically, so continuous observations are needed to monitor how this flux has evolved and will evolve in the future.

The South Shetland margin (north-west of the Antarctic Peninsula), is the most studied region with respect to gas hydrates in the Southern Ocean (Giustiniani & Tinivella, 2021) where the presence of marine CH_4 hydrate reservoirs have been inferred by seismic studies (Jin et al., 2003; Loreto et al., 2010; Marín-Moreno et al., 2015). It is also thought that the seabed waters around the Antarctic Peninsula may be cold enough to support the development of CH_4 hydrates at shallower depths, as seen in the Arctic (Marín-Moreno et al., 2015). On the east side of the Peninsula, del Valle et al. (2017) observed bubbling of CH_4 from the seafloor next to Seymour Island, Weddell Sea, suggesting a presence of gas accumulation in marine sediments in the area. The waters around the West Antarctic Peninsula are currently displaying some of the most substantial warming in the Southern Ocean (Fox-Kemper et al., 2021), with warming of both the upper and deeper ocean (Meredith & King, 2005), which raises the question if this could lead to dissociation of hydrates in the these waters and a release of CH_4. Additionally, the increasing air temperatures around the Antarctic Peninsula could lead to accelerated melting of glaciers in this area, leading to elevated outflow of subglacial, CH_4-enriched waters into coastal areas in the region.

The findings of this study provide potential indications of CH_4 originating from the seabed penetrating the sea-air interface in the South Shetland Islands, there are clusters of elevated sea-air CH_4 fluxes in specific areas coinciding with evidence of seabed CH_4 seepage. For example, there are six fluxes above LoD in the bay of Deception Island, where we also find evidence of flares in the water column. Deception Island is a caldera of an active volcano, therefore there is potentially a hydrothermal source of the CH_4 (Tilbrook & Karl, 1993). Tilbrook and Karl (1993) found that the waters in Deception Island are supersaturated with CH_4, with surface concentrations three times higher than found during the same campaign in the Drake Passage, Bransfield Strait and Gerlache Strait. In Deception Island, the surface concentration was equivalent to a saturation ratio of 3.17, indicating that this area is a source of atmospheric CH_4. Additionally, the study found elevated concentrations throughout the water column, with the higher concentrations closer to the seabed (150 m bsl). A flare was detected in the caldera of Deception Island using EK60 data collected on a previous *JCR* cruise (JR17002) on 20/01/2018 (Figure 5b), providing evidence of seabed seepage in this region. Considering these factors, it is likely that there is a seabed source of CH_4 in the caldera of Deception Island, and hence the elevated CH_4 flux into the atmosphere may be of seabed origin. There is a cluster of 13 elevated fluxes in Marian Cove, King George Island. We find streams of single bubbles rising from the seabed in Admiralty Bay, King George Island from cruise RRS *Sir David Attenborough (SDA)* SDA025 on 25/02/2023 (Figure 5c), while this is a different bay from the bay with the elevated sea-air fluxes, it provides potential evidence of the existence of CH_4 seepage from the seabed around King George Island. Therefore, there may also be seabed seepage present in Marian Cove, if we assume same geological processes/conditions are present in each bay. It is also important to note that the elevated fluxes in Marian Cove and Deception Island may also be attributed to subglacial outflow of CH_4 enriched waters (Andrews, 2019; Christiansen & Jørgensen, 2018; Lamarche-Gagnon et al., 2019), as there is a marine terminating glacier flowing directly into Marian Cove, and there are many glaciers flowing into the bay of Deception Island.

Around the South Shetland Islands there are clusters of elevated sea-air CH_4 fluxes in places where seabed seeps are likely to be found, and in regions where elevated CH_4 concentrations throughout the water column have been found before. This indicates that seabed produced CH_4 likely can make it to the atmosphere in places with the appropriate conditions. Additionally, our results reveal sea-air fluxes in this region that are one to two orders of magnitude larger than observed approximately 30 years prior in the same area, suggesting a significant increase in the quantity of CH_4 released into the atmosphere from these waters. However, it is unclear what impact the measurement method plays in the discrepancies between this study and (Tilbrook & Karl, 1994). Using eddy-covariance method it is not possible to distinguish the process by which CH_4 reaches the atmosphere - eddy-covariance can't discriminate between direct emission (e.g., ebullition) or diffusion of dissolved CH_4, although this could be achieved with a different experimental set up.

5. Conclusion

This study is the first to our knowledge to investigate sea-air CH_4 fluxes using the eddy-covariance method in both the Southern Ocean and Arctic Ocean. We find that on-shelf regions in both the Southern Ocean and the Arctic Ocean are sources of CH_4 to the atmosphere, with the mean on-shelf fluxes being the same for both oceans, within the margin of error. This may imply that similar processes are governing the on-shelf release of CH_4 in both oceans. In contrast, the off-shelf regions of the Arctic Ocean act as sources of atmospheric CH_4, whereas those in the Southern Ocean act as sinks. This discrepancy between the off-shelf areas of the two oceans may arise from the strong upwelling present in the Southern Ocean, which transports deeper, CH_4 depleted waters to the surface.

The sea-air CH_4 eddy-covariance flux data set is noisy, and relatively few fluxes lie above LoD. There are several clusters of fluxes above the LoD: Western Svalbard (Arctic Ocean) and South Georgia and the South Shetland Islands and Bransfield Strait (Southern Ocean). Seabed CH_4 seepage has been identified at or near each of these locations by this study and by previous studies. Therefore, the findings of this study may provide evidence of seabed produced CH_4 reaching the atmosphere. Previous studies have found that seeps off the west coast of Svalbard do not have an impact on the atmospheric CH_4 concentration. Even though we do not analysis atmospheric concentrations in this study, our study is significant as we do find that increased emission of CH_4 into the atmosphere, compared to other areas. Outflow of CH_4-enriched freshwater from the land (i.e., in proglacial streams) could also play a factor in the elevated CH_4 flux around the coastal areas in the Arctic and Antarctic. The Arctic Ocean (and Svalbard) is better studied in regards to CH_4 and sea-air CH_4 fluxes than the Southern Ocean,

so this research offers valuable insights into the role the Southern Ocean plays in the atmospheric CH_4 cycle, and how it is changing. The results of this study imply that the amount of CH_4 released from coastal areas with known seabed seeps in the Southern Ocean has increased over the last few decades, from when it was last studied in the late 1980s (Tilbrook & Karl, 1994). If the rapid warming of the waters around the Antarctic Peninsula continues into the future, there could be lasting and future impacts on the carbon stored in the marine sediments, and hence the amount of CH_4 released into the atmosphere from these waters. Additionally, the impact of freshwater outflow on the quantity of CH_4 released from coastal areas in this region could be amplified due to climate warming leading to increased melting of terrestrial ice. This study highlights the need for continued monitoring of sea-air CH_4 fluxes, as well as CH_4 in the water column and in the seabed sediments around the Antarctic Peninsula. Future work pairing water column data (dissolved CH_4 concentration, salinity, temperature, acoustics) together with eddy-covariance data would allow a more comprehensive study of the sources of CH_4 in this region and the pathways to the atmosphere. This work demonstrates the feasibility of using eddy-covariance to measure sea-air CH_4 fluxes over the oceans, and continued ship based monitoring in the polar regions is important to allow enough data so that robust trends can be elucidated.

Data Availability Statement

The processed two hourly CH_4 sea-air eddy-covariance data used in this study for analyzing CH_4 fluxes from oceans is available at the UK Polar Data Centre (PDC) (Workman et al., 2024). The EK60 and EK80 data used in this study is available at the PDC (Fielding, 2024a, 2024b; Fielding & Manno, 2024).

Acknowledgments
This work was supported by the Natural Environment Research Council and the ARIES Doctoral Training Partnership (Grant NE/S007334/1). We would like to thank the masters, nautical officers, and all crew members of the research vessel RRS James Clark Ross (JR18004- JR18007, JR19001, JR19002, Logistics01 and Logistics02), especially the deck's engineers who looked after the Picarro G2311-f. Royal Holloway, University of London thanks NERC for funding through Grants NE/V000780/1 and NE/N016211/1. Anna E. Jones and Katrin Linse were part of the British Antarctic Survey Polar Science for Planet Earth Programme funded by The Natural Environment Research Council (NERC). The measurements from the Royal Research Ship James Clark Ross (JCR) were principally supported by the UK Natural Environment Research Council's ORCHESTRA project (Grant NE/N018095/1). The Picarro analyzer was funded by the European Space Agency funding (ESA AMT4OceanSatFlux project, Grant 4000125730/18/NL/FF/gp). This work further contributes to the NERC MOYA project (Grant NE/N015932/1). We would like to thank Clara Manno (PSO of JR17002) and Sophie Fielding (PSO of JR19001 and SDA 025) for providing the acoustic data analyzed in this study and making it open access. We would like to thank the three anonymous reviewers for taking time to give valuable comments and suggestions which have improved this paper.

References

Andrews, L. C. (2019). Methane beneath Greenland's ice sheet is being released. *Nature*, *565*(7737), 31–32. https://doi.org/10.1038/d41586-018-07762-7

Angelopoulos, M., Overduin, P. P., Miesner, F., Grigoriev, M. N., & Vasiliev, A. A. (2020). Recent advances in the study of Arctic submarine permafrost. *Permafrost and Periglacial Processes*, *31*(3), 442–453. https://doi.org/10.1002/ppp.2061

Bange, H. W., Bartell, U. H., Rapsomanikis, S., & Andreae, M. O. (1994). Methane in the Baltic and North Seas and a reassessment of the marine emissions of methane. *Global Biogeochemical Cycles*, *8*(4), 465–480. https://doi.org/10.1029/94gb02181

Barnes, R. O., & Goldberg, E. D. (1976). Methane production and consumption in anoxic marine sediments. *Geology*, *4*(5), 297. https://doi.org/10.1130/0091-7613(1976)4<297:mpacia>2.0.co;2

Bastviken, D., Cole, J., Pace, M., & Tranvik, L. (2004). Methane emissions from lakes: Dependence of lake characteristics, two regional assessments, and a global estimate. *Global Biogeochemical Cycles*, *18*(4), GB4009. https://doi.org/10.1029/2004GB002238

Beaulieu, J. J., DelSontro, T., & Downing, J. A. (2019). Eutrophication will increase methane emissions from lakes and impoundments during the 21st century. *Nature Communications*, *10*(1), 1375. https://doi.org/10.1038/s41467-019-09100-5

Berndt, C., Feseker, T., Treude, T., Krastel, S., Liebetrau, V., Niemann, H., et al. (2014). Temporal constraints on hydrate-controlled methane seepage off Svalbard. *Science*, *343*(6168), 284–287. https://doi.org/10.1126/science.1246298

Bertora, C., Cucu, M. A., Lerda, C., Peyron, M., Bardi, L., Gorra, R., et al. (2018). Dissolved organic carbon cycling, methane emissions and related microbial populations in temperate rice paddies with contrasting straw and water management. *Agriculture, Ecosystems & Environment*, *265*, 292–306. https://doi.org/10.1016/j.agee.2018.06.004

Betlem, P., Roy, S., Birchall, T., Hodson, A., Noormets, R., Römer, M., et al. (2021). Modelling of the gas hydrate potential in Svalbard's fjords. *Journal of Natural Gas Science and Engineering*, *94*, 104127. https://doi.org/10.1016/j.jngse.2021.104127

Biastoch, A., Treude, T., Rüpke, L. H., Riebesell, U., Roth, C., Burwicz, E. B., et al. (2011). Rising Arctic Ocean temperatures cause gas hydrate destabilization and ocean acidification. *Geophysical Research Letters*, *38*(8), L08602. https://doi.org/10.1029/2011gl047222

Bohrmann, G., Aromokeye, A. D., Bihler, V., Dehning, K., Dohrmann, I., Gentz, T., et al. (2017). R/V METEOR cruise report M134, emissions of free gas from cross-shelf troughs of South Georgia: Distribution, quantification, and sources for methane ebullition Sites in Sub-Antarctic waters. *Port Stanley (Falkland Islands) – Punta Arenas (Chile), 16 January – 18 February 2017 (Tech. Rep.)*.

Bohrmann, G., Ferreira, H., Hsu, W.-L., Lange, C.-W., Loher, M., Pape, M., et al. (2015). R/V HEINCKE cruise report HE450 dynamics of gas emissions along the Barents Sea Svalbard margin (Tech. Rep.).

Borges, A. V., Champenois, W., Gypens, N., Delille, B., & Harlay, J. (2016). Massive marine methane emissions from near-shore shallow coastal areas. *Scientific Reports*, *6*(1), 27908. https://doi.org/10.1038/srep27908

Borrel, G., Jézéquel, D., Biderre-Petit, C., Morel-Desrosiers, N., Morel, J.-P., Peyret, P., et al. (2011). Production and consumption of methane in freshwater lake ecosystems. *Research in Microbiology*, *162*(9), 832–847. https://doi.org/10.1016/j.resmic.2011.06.004

Boyd, E. S., Skidmore, M., Mitchell, A. C., Bakermans, C., & Peters, J. W. (2010). Methanogenesis in subglacial sediments. *Environmental Microbiology Reports*, *2*(5), 685–692. https://doi.org/10.1111/j.1758-2229.2010.00162.x

Brusselman, A., Crabeck, O., Muller, S., Araujo, P. A., Dogniez, M., Lepoint, G., et al. (2024). Glacier meltwater, a potential source of methane in West Antarctica Peninsula. In *EGU general assembly 2024* (pp. egu24–18144). https://doi.org/10.5194/egusphere-egu24-18144

Bui, O. T. N., Kameyama, S., Yoshikawa-Inoue, H., Ishii, M., Sasano, D., Uchida, H., & Tsunogai, U. (2018). Estimates of methane emissions from the Southern Ocean from quasi-continuous underway measurements of the partial pressure of methane in surface seawater during the 2012/13 austral summer. *Tellus Series B Chemical and Physical Meteorology*, *70*(1), 1–15. https://doi.org/10.1080/16000889.2018.1478594

Burns, R., Wynn, P. M., Barker, P., McNamara, N., Oakley, S., Ostle, N., et al. (2018). Direct isotopic evidence of biogenic methane production and efflux from beneath a temperate glacier. *Scientific Reports*, *8*(1), 17118. https://doi.org/10.1038/s41598-018-35253-2

Christiansen, J. R., & Jørgensen, C. J. (2018). First observation of direct methane emission to the atmosphere from the subglacial domain of the Greenland Ice Sheet. *Scientific Reports*, *8*(1), 16623. https://doi.org/10.1038/s41598-018-35054-7

Colleoni, F., De Santis, L., Montoli, E., Olivo, E., Sorlien, C. C., Bart, P. J., et al. (2018). Past continental shelf evolution increased Antarctic ice sheet sensitivity to climatic conditions. *Scientific Reports*, *8*(1), 11323. https://doi.org/10.1038/s41598-018-29718-7

Damm, E., Mackensen, A., Budéus, G., Faber, E., & Hanfland, C. (2005). Pathways of methane in seawater: Plume spreading in an Arctic shelf environment (SW-Spitsbergen). *Continental Shelf Research*, *25*(12–13), 1453–1472. https://doi.org/10.1016/j.csr.2005.03.003

Damm, E., Schauer, U., Rudels, B., & Haas, C. (2007). Excess of bottom-released methane in an Arctic shelf sea polynya in winter. *Continental Shelf Research*, *27*(12), 1692–1701. https://doi.org/10.1016/j.csr.2007.02.003

del Valle, R. A., Yermolin, E., Chiarandini, J., Granel, A. S., & Lusky, J. C. (2017). Methane at the NW of Weddell Sea, Antarctica. *Journal of Geological Research*, *2017*, 1–8. https://doi.org/10.1155/2017/5952916

Dickens, G. R., ONeil, J. R., Rea, D. K., & Owen, R. M. (1995). Dissociation of oceanic methane hydrate as a cause of the carbon isotope excursion at the end of the Paleocene. *Paleoceanography*, *10*(6), 965–971. https://doi.org/10.1029/95pa02087

Dølven, K. O., Ferré, B., Silyakova, A., Jansson, P., Linke, P., & Moser, M. (2022). Autonomous methane seep site monitoring offshore western Svalbard: Hourly to seasonal variability and associated oceanographic parameters. *Ocean Science*, *18*(1), 233–254. https://doi.org/10.5194/os-18-233-2022

Dong, Y., Yang, M., Bakker, D. C., Liss, P. S., Kitidis, V., Brown, I., et al. (2021). Near-surface stratification due to ice melt biases Arctic Air-Sea CO_2 flux estimates. *Geophysical Research Letters*, *48*(22). https://doi.org/10.1029/2021GL095266

Dong, Y., Yang, M., Bakker, D. C. E., Kitidis, V., & Bell, T. G. (2021). Uncertainties in eddy covariance airsea CO_2 flux measurements and implications for gas transfer velocity parameterisations. *Atmospheric Chemistry and Physics*, *21*(10), 8089–8110. https://doi.org/10.5194/acp-21-8089-2021

Dorschel, B., Hehemann, L., Viquerat, S., Warnke, F., Dreutter, S., Tenberge, Y. S., et al. (2022). The international bathymetric chart of the Southern Ocean version 2. *Scientific Data*, *9*(1), 1–13. https://doi.org/10.1038/s41597-022-01366-7

Emery, K. O. (1969). The continental shelves. *Scientific American*, *221*(3), 106–125. https://doi.org/10.2307/26069611

Fenwick, L., Capelle, D., Damm, E., Zimmermann, S., Williams, W. J., Vagle, S., & Tortell, P. D. (2017). Methane and nitrous oxide distributions across the North American Arctic Ocean during summer, 2015. *Journal of Geophysical Research: Oceans*, *122*(1), 390–412. https://doi.org/10.1002/2016jc012493

Ferré, B., Jansson, P. G., Moser, M., Serov, P., Portnov, A., Graves, C. A., et al. (2020). Reduced methane seepage from Arctic sediments during cold bottom-water conditions. *Nature Geoscience*, *13*(2), 144–148. https://doi.org/10.1038/s41561-019-0515-3

Fielding, S. (2024a). Raw acoustic data collected by an EK60 echosounder at South Georgia Island on board the RRS James Clark Ross cruise JR19001 (10 December 2019). https://doi.org/10.5285/8ef97c2d-9ce6-4ddc-ba63-28c47b6cc147

Fielding, S. (2024b). Raw acoustic data collected by an EK80 echosounder at King George Island on board the RRS Sir David Attenborough cruise SD025 (25 February 2023). https://doi.org/10.5285/e7c3f05f-7677-408c-b98d-d35bd2171550

Fielding, S., & Manno, C. (2024). Raw acoustic data collected by an EK60 echosounder in Bransfield Strait and the caldera of Deception Island on board the RRS James Clark Ross cruise JR17002 (20 January 2018). https://doi.org/10.5285/0826a8a0-e9c5-4504-8f75-a7516041c282

Fisher, R. E., Sriskantharajah, S., Lowry, D., Lanoisellé, M., Fowler, C. M. R., James, R. H., et al. (2011). Arctic methane sources: Isotopic evidence for atmospheric inputs. *Geophysical Research Letters*, *38*(21), L21803. https://doi.org/10.1029/2011gl049319

Formolo, M. (2010). The microbial production of methane and other volatile hydrocarbons. In *Handbook of hydrocarbon and lipid microbiology* (pp. 113–126). Springer Berlin Heidelberg. https://doi.org/10.1007/978-3-540-77587-4{_}6

Forster, P., Storelvmo, T., Armour, K., Collins, W., Dufresne, J.-L., Frame, D., et al. (2021). The Earth's energy budget, climate feedbacks, and climate sensitivity. In V. Masson-Delmotte, et al. (Eds.), *Climate change 2021: The physical science basis. contribution of working group i to the sixth assessment report of the intergovernmental panel on climate change (chap. 7)*. https://doi.org/10.1017/9781009157896.009

Fox-Kemper, B., Hewitt, H. T., Xiao, C., Að algeirsdóttir, G., Drijfhout, S. S., Edwards, T. L., et al. (2021). Ocean, cryosphere and sea level change. In V. Masson-Delmotte, et al. (Eds.), *Climate change 2021: The physical science basis. contribution of working group I to the sixth assessment report of the intergovernmental panel on climate change (chap. 9)*. Cambridge University Press. https://doi.org/10.1017/9781009157896.011

GEBCO Compilation Group. (2023). GEBCO_2023 grid.

Geissler, W. H., Gebhardt, A. C., Gross, F., Wollenburg, J., Jensen, L., Schmidt-Aursch, M. C., et al. (2016). Arctic megaslide at presumed rest. *Scientific Reports*, *6*(1), 38529. https://doi.org/10.1038/srep38529

Geprägs, P., Torres, M. E., Mau, S., Kasten, S., Römer, M., & Bohrmann, G. (2016). Carbon cycling fed by methane seepage at the shallow Cumberland Bay, South Georgia, sub-Antarctic. *Geochemistry, Geophysics, Geosystems*, *17*(4), 1401–1418. https://doi.org/10.1002/2016GC006276

Giustiniani, M., & Tinivella, U. (2021). Gas hydrates in Antarctica. In *Glaciers and the polar environment*. IntechOpen. https://doi.org/10.5772/intechopen.94306

Graves, C. A., Steinle, L., Rehder, G., Niemann, H., Connelly, D. P., Lowry, D., et al. (2015). Fluxes and fate of dissolved methane released at the seafloor at the landward limit of the gas hydrate stability zone offshore western Svalbard. *Journal of Geophysical Research: Oceans*, *120*(9), 6185–6201. https://doi.org/10.1002/2015jc011084

Hanson, R. S., & Hanson, T. E. (1996). Methanotrophic bacteria. *Microbiological Reviews*, *60*(2), 439–471. https://doi.org/10.1128/mr.60.2.439-471.1996

Hartman, W. H., Bueno de Mesquita, C. P., Theroux, S. M., Morgan-Lang, C., Baldocchi, D. D., & Tringe, S. G. (2024). Multiple microbial guilds mediate soil methane cycling along a wetland salinity gradient. *mSystems*, *9*(1). https://doi.org/10.1128/msystems.00936-23

Heeschen, K. U., Keir, R. S., Rehder, G., Klatt, O., & Suess, E. (2004). Methane dynamics in the Weddell Sea determined via stable isotope ratios and CFC-11. *Global Biogeochemical Cycles*, *18*(2), GB2012. https://doi.org/10.1029/2003gb002151

Hester, K. C., & Brewer, P. G. (2009). Clathrate hydrates in nature. *Annual Review of Marine Science*, *1*(1), 303–327. https://doi.org/10.1146/annurev.marine.010908.163824

Heywood, K. J., Schmidtko, S., Heuzé, C., Kaiser, J., Jickells, T. D., Queste, B. Y., et al. (2014). Ocean processes at the Antarctic continental slope. *Philosophical Transactions of the Royal Society A: Mathematical, Physical & Engineering Sciences*, *372*(2019), 20130047. https://doi.org/10.1098/rsta.2013.0047

Hinrichs, K.-U., & Boetius, A. (2002). The anaerobic oxidation of methane: New insights in microbial ecology and biogeochemistry. In *Ocean margin systems* (pp. 457–477). Springer Berlin Heidelberg. https://doi.org/10.1007/978-3-662-05127-6{_}28

Hodson, A. J., Nowak, A., Hornum, M. T., Senger, K., Redeker, K., Christiansen, H. H., et al. (2020). Sub-permafrost methane seepage from open-system pingos in Svalbard. *The Cryosphere*, *14*(11), 3829–3842. https://doi.org/10.5194/tc-14-3829-2020

Hunter, S. J., Goldobin, D. S., Haywood, A. M., Ridgwell, A., & Rees, J. G. (2013). Sensitivity of the global submarine hydrate inventory to scenarios of future climate change. *Earth and Planetary Science Letters*, *367*, 105–115. https://doi.org/10.1016/j.epsl.2013.02.017

James, R. H., Bousquet, P., Bussmann, I., Haeckel, M., Kipfer, R., Leifer, I., et al. (2016). Effects of climate change on methane emissions from seafloor sediments in the Arctic Ocean: A review. *Limnology & Oceanography*, *61*(S1). https://doi.org/10.1002/lno.10307

Jin, Y. K., Lee, M. W., Kim, Y., Nam, S. H., & Kim, K. J. (2003). Gas hydrate volume estimations on the South Shetland continental margin, Antarctic Peninsula. *Antarctic Science*, *15*(2), 271–282. https://doi.org/10.1017/S0954102003001275

Joung, D., Ruppel, C., Southon, J., Weber, T. S., & Kessler, J. D. (2022). Negligible atmospheric release of methane from decomposing hydrates in mid-latitude oceans. *Nature Geoscience*, *15*(11), 885–891. https://doi.org/10.1038/s41561-022-01044-8

Judd, A. G., Hovland, M., Dimitrov, L. I., Gil, S. G., & Jukes, V. (2002). The geological methane budget at Continental Margins and its influence on climate change. *Geofluids*, *2*(2), 109–126. https://doi.org/10.1046/j.1468-8123.2002.00027.x

Karion, A., Sweeney, C., Pétron, G., Frost, G., Hardesty, R. M., Kofler, J., et al. (2013). Methane emissions estimate from airborne measurements over a western United States natural gas field. *Geophysical Research Letters*, *40*(16), 4393–4397. https://doi.org/10.1002/grl.50811

Kleber, G. E., Hodson, A. J., Magerl, L., Mannerfelt, E. S., Bradbury, H. J., Zhu, Y., et al. (2023). Groundwater springs formed during glacial retreat are a large source of methane in the high Arctic. *Nature Geoscience*, *16*(7), 597–604. https://doi.org/10.1038/s41561-023-01210-6

Knies, J., Damm, E., Gutt, J., Mann, U., & Pinturier, L. (2004). Near-surface hydrocarbon anomalies in shelf sediments off Spitsbergen: Evidences for past seepages. *Geochemistry, Geophysics, Geosystems*, *5*(6), Q06003. https://doi.org/10.1029/2003gc000687

Kongsberg. (2023). EK80 software. Retrieved from https://www.kongsberg.com/maritime/products/ocean-science/ocean-science/es_scientific/ek80software/

Kretschmer, K., Biastoch, A., Rüpke, L., & Burwicz, E. (2015). Modeling the fate of methane hydrates under global warming. *Global Biogeochemical Cycles*, *29*(5), 610–625. https://doi.org/10.1002/2014gb005011

Kvenvolden, K. A. (1988). Methane hydrate A major reservoir of carbon in the shallow geosphere? *Chemical Geology*, *71*(1–3), 41–51. https://doi.org/10.1016/0009-2541(88)90104-0

Kvenvolden, K. A. (1993). Gas hydrates-geological perspective and global change. *Reviews of Geophysics*, *31*(2), 173–187. https://doi.org/10.1029/93rg00268

Lamarche-Gagnon, G., Wadham, J. L., Sherwood Lollar, B., Arndt, S., Fietzek, P., Beaton, A. D., et al. (2019). Greenland melt drives continuous export of methane from the ice-sheet bed. *Nature*, *565*(7737), 73–77. https://doi.org/10.1038/s41586-018-0800-0

Lan, X., Thoning, K., & Dlugokencky, E. (2023). Trends in globally-averaged CH_4, N_2O, and SF_6 determined from NOAA global monitoring laboratory measurements. Version 2023-12. https://doi.org/10.15138/P8XG-AA10

Leonte, M., Ruppel, C. D., Ruiz-Angulo, A., & Kessler, J. D. (2020). Surface methane concentrations along the mid-atlantic bight driven by aerobic subsurface production rather than seafloor gas seeps. *Journal of Geophysical Research: Oceans*, *125*(5), e2019JC015989. https://doi.org/10.1029/2019jc015989

Liss, P. S. (1973). Processes of gas exchange across an air-water interface (Vol. *20*). (Tech. Rep.).

Loreto, M. F., Tinivella, U., Accaino, F., & Giustiniani, M. (2010). Offshore Antarctic Peninsula gas hydrate reservoir characterization by geophysical data analysis. *Energies*, *4*(1), 39–56. https://doi.org/10.3390/en4010039

Marín-Moreno, H., Giustiniani, M., & Tinivella, U. (2015). The potential response of the hydrate reservoir in the South Shetland Margin, Antarctic Peninsula, to ocean warming over the 21st century. *Polar Research*, *34*(1), 27443. https://doi.org/10.3402/polar.v34.27443

Marín-Moreno, H., Minshull, T. A., Westbrook, G. K., Sinha, B., & Sarkar, S. (2013). The response of methane hydrate beneath the seabed offshore Svalbard to ocean warming during the next three centuries. *Geophysical Research Letters*, *40*(19), 5159–5163. https://doi.org/10.1002/grl.50985

Mau, S., Römer, M., Torres, M. E., Bussmann, I., Pape, T., Damm, E., et al. (2017). Widespread methane seepage along the continental margin off Svalbard - From Bjørnøya to Kongsfjorden. *Scientific Reports*, *7*(1), 42997. https://doi.org/10.1038/srep42997

McGinnis, D. F., Greinert, J., Artemov, Y., Beaubien, S. E., & Wüest, A. (2006). Fate of rising methane bubbles in stratified waters: How much methane reaches the atmosphere? *Journal of Geophysical Research*, *111*(C9), C09007. https://doi.org/10.1029/2005jc003183

Meredith, M. P., & King, J. C. (2005). Rapid climate change in the ocean west of the Antarctic Peninsula during the second half of the 20th century. *Geophysical Research Letters*, *32*(19), L19604. https://doi.org/10.1029/2005gl024042

Murrell, J. C. (2010). The aerobic methane oxidizing bacteria (methanotrophs). In *Handbook of hydrocarbon and lipid microbiology* (pp. 1953–1966). Springer Berlin Heidelberg. https://doi.org/10.1007/978-3-540-77587-4{_}143

Myhre, C. L., Ferré, B., Platt, S. M., Silyakova, A., Hermansen, O., Allen, G., et al. (2016). Extensive release of methane from Arctic seabed west of Svalbard during summer 2014 does not influence the atmosphere. *Geophysical Research Letters*, *43*(9), 4624–4631. https://doi.org/10.1002/2016gl068999

Pisso, I., Myhre, C. L., Platt, S. M., Eckhardt, S., Hermansen, O., Schmidbauer, N., et al. (2016). Constraints on oceanic methane emissions west of Svalbard from atmospheric in situ measurements and Lagrangian transport modeling. *Journal of Geophysical Research: Atmospheres*, *121*(23), 14188–14200. https://doi.org/10.1002/2016jd025590

Platt, S. M., Eckhardt, S., Ferré, B., Fisher, R. E., Hermansen, O., Jansson, P., et al. (2018). Methane at Svalbard and over the European Arctic Ocean. *Atmospheric Chemistry and Physics*, *18*(23), 17207–17224. https://doi.org/10.5194/acp-18-17207-2018

Punshon, S., Azetsu-Scott, K., & Lee, C. M. (2014). On the distribution of dissolved methane in Davis Strait, North Atlantic Ocean. *Marine Chemistry*, *161*, 20–25. https://doi.org/10.1016/j.marchem.2014.02.004

Rajan, A., Mienert, J., & Bünz, S. (2012). Acoustic evidence for a gas migration and release system in Arctic glaciated continental margins offshore NW-Svalbard. *Marine and Petroleum Geology*, *32*(1), 36–49. https://doi.org/10.1016/j.marpetgeo.2011.12.008

Reeburgh, W. S. (1980). Anaerobic methane oxidation: Rate depth distributions in Skan Bay sediments. *Earth and Planetary Science Letters*, *47*(3), 345–352. https://doi.org/10.1016/0012-821x(80)90021-7

Reeburgh, W. S. (2007). Oceanic methane biogeochemistry. *Chemical Reviews*, *107*(2), 486–513. https://doi.org/10.1021/cr050362v

Rehder, G., Keir, R. S., Suess, E., & Pohlmann, T. (1998). The multiple sources and patterns of methane in North Sea waters. *Aquatic Geochemistry*, *4*(3/4), 403–427. https://doi.org/10.1023/a:1009644600833

Römer, M., Torres, M., Kasten, S., Kuhn, G., Graham, A. G. C., Mau, S., et al. (2014). First evidence of widespread active methane seepage in the Southern Ocean, off the sub-Antarctic island of South Georgia. *Earth and Planetary Science Letters*, *403*, 166–177. https://doi.org/10.1016/j.epsl.2014.06.036

Roy, S., Senger, K., Hovland, M., Römer, M., & Braathen, A. (2019). Geological controls on shallow gas distribution and seafloor seepage in an Arctic fjord of Spitsbergen, Norway. *Marine and Petroleum Geology*, *107*, 237–254. https://doi.org/10.1016/j.marpetgeo.2019.05.021

Ruppel, C. D. (2011). Methane hydrates and contemporary climate change. *Nature Education Knowledge*, *3*(10), 29.

Ruppel, C. D., & Kessler, J. D. (2017). The interaction of climate change and methane hydrates. *Reviews of Geophysics*, *55*(1), 126–168. https://doi.org/10.1002/2016rg000534

Sahling, H., Römer, M., Pape, T., Bergès, B., dos Santos Fereirra, C., Boelmann, J., et al. (2014). Gas emissions at the continental margin west of Svalbard: Mapping, sampling, and quantification. *Biogeosciences*, *11*(21), 6029–6046. https://doi.org/10.5194/bg-11-6029-2014

Saunois, M., Stavert, A. R., Poulter, B., Bousquet, P., Canadell, J. G., Jackson, R. B., et al. (2020). The global methane budget 20002017. *Earth System Science Data*, *12*(3), 1561–1623. https://doi.org/10.5194/essd-12-1561-2020

Scranton, M. I., & McShane, K. (1991). Methane fluxes in the southern North Sea: The role of European rivers. *Continental Shelf Research*, *11*(1), 37–52. https://doi.org/10.1016/0278-4343(91)90033-3

Seabrook, S., Thurber, A., Ladroit, Y., Discovery, K., Cummings, V., Tait, L., et al. (2023). Emergent Antarctic seafloor seeps: A tipping point reached? https://doi.org/10.21203/rs.3.rs-3657723/v1

Shakhova, N., & Semiletov, I. (2007). Methane release and coastal environment in the East Siberian Arctic shelf. *Journal of Marine Systems*, *66*(1–4), 227–243. https://doi.org/10.1016/j.jmarsys.2006.06.006

Shakhova, N., Semiletov, I., Leifer, I., Sergienko, V., Salyuk, A., Kosmach, D., et al. (2014). Ebullition and storm-induced methane release from the East Siberian Arctic Shelf. *Nature Geoscience*, *7*(1), 64–70. https://doi.org/10.1038/ngeo2007

Shakhova, N., Semiletov, I., Sergienko, V., Lobkovsky, L., Yusupov, V., Salyuk, A., et al. (2015). The East Siberian Arctic Shelf: Towards further assessment of permafrost-related methane fluxes and role of sea ice. *Philosophical Transactions of the Royal Society A: Mathematical, Physical & Engineering Sciences*, *373*(2052), 20140451. https://doi.org/10.1098/rsta.2014.0451

Skarke, A., Ruppel, C., Kodis, M., Brothers, D., & Lobecker, E. (2014). Widespread methane leakage from the sea floor on the northern US Atlantic margin. *Nature Geoscience*, *7*(9), 657–661. https://doi.org/10.1038/ngeo2232

Steinle, L., Graves, C. A., Treude, T., Ferré, B., Biastoch, A., Bussmann, I., et al. (2015). Water column methanotrophy controlled by a rapid oceanographic switch. *Nature Geoscience*, *8*(5), 378–382. https://doi.org/10.1038/ngeo2420

Stibal, M., Wadham, J. L., Lis, G. P., Telling, J., Pancost, R. D., Dubnick, A., et al. (2012). Methanogenic potential of Arctic and Antarctic subglacial environments with contrasting organic carbon sources. *Global Change Biology*, *18*(11), 3332–3345. https://doi.org/10.1111/j.1365-2486.2012.02763.x

Thornton, B. F., Geibel, M. C., Crill, P. M., Humborg, C., & Mörth, C.-M. (2016). Methane fluxes from the sea to the atmosphere across the Siberian shelf seas. *Geophysical Research Letters*, *43*(11), 5869–5877. https://doi.org/10.1002/2016gl068977

Thornton, B. F., Prytherch, J., Andersson, K., Brooks, I. M., Salisbury, D., Tjernström, M., & Crill, P. M. (2020). Shipborne eddy covariance observations of methane fluxes constrain Arctic sea emissions. *Science Advances*, *6*(5). https://doi.org/10.1126/sciadv.aay7934

Thurber, A. R., Seabrook, S., & Welsh, R. M. (2020). Riddles in the cold: Antarctic endemism and microbial succession impact methane cycling in the Southern Ocean. *Proceedings of the Royal Society B: Biological Sciences*, *287*(1931), 20201134. https://doi.org/10.1098/rspb.2020.1134

Tilbrook, B. D., & Karl, D. M. (1993). RACER: Methane enrichments in Port Foster, Deception Island (Tech. Rep.).

Tilbrook, B. D., & Karl, D. M. (1994). Dissolved methane distributions, sources, and sinks in the western Bransfield Strait, Antarctica. *Journal of Geophysical Research*, *99*(C8), 16383–16393. https://doi.org/10.1029/94jc01043

Upstill-Goddard, R. C., Barnes, J., Frost, T., Punshon, S., & Owens, N. J. P. (2000). Methane in the southern North Sea: Low-salinity inputs, estuarine removal, and atmospheric flux. *Global Biogeochemical Cycles*, *14*(4), 1205–1217. https://doi.org/10.1029/1999gb001236

Veloso, M., Greinert, J., Mienert, J., & Batist, M. D. (2019). Corrigendum: A new methodology for quantifying bubble flow rates in deep water using splitbeam echosounders: Examples from the Arctic offshore NW-Svalbard. *Limnology and Oceanography: Methods*, *17*(2), 177–178. https://doi.org/10.1002/lom3.10313

Vogt, J., Risk, D., Bourlon, E., Azetsu-Scott, K., Edinger, E. N., & Sherwood, O. A. (2023). Sea–air methane flux estimates derived from marine surface observations and instantaneous atmospheric measurements in the northern Labrador Sea and Baffin Bay. *Biogeosciences*, *20*(9), 1773–1787. https://doi.org/10.5194/bg-20-1773-2023

Wang, B., Socolofsky, S. A., Breier, J. A., & Seewald, J. S. (2016). Observations of bubbles in natural seep flares at MC 118 and GC 600 using in situ quantitative imaging. *Journal of Geophysical Research: Oceans*, *121*(4), 2203–2230. https://doi.org/10.1002/2015jc011452

Weber, T., Wiseman, N. A., & Kock, A. (2019). Global ocean methane emissions dominated by shallow coastal waters. *Nature Communications*, *10*(1), 4584. https://doi.org/10.1038/s41467-019-12541-7

Westbrook, G. K., Thatcher, K. E., Rohling, E. J., Piotrowski, A. M., Pälike, H., Osborne, A. H., et al. (2009). Escape of methane gas from the seabed along the West Spitsbergen continental margin. *Geophysical Research Letters*, *36*(15), L15608. https://doi.org/10.1029/2009gl039191

Whiticar, M. J. (1999). Carbon and hydrogen isotope systematics of bacterial formation and oxidation of methane. *Chemical Geology*, *161*(1–3), 291–314. https://doi.org/10.1016/s0009-2541(99)00092-3

Workman, E., Yang, M., Bell, T., Dong, Y., Jones, A., Fisher, R., et al. (2024). *Sea-air methane fluxes measured using an eddy-covariance technique on RRS James Clark Ross from January 2019 to March 2021 (version 1.0)*. NERC EDS UK Polar Data Centre. https://doi.org/10.5285/c9ed4746-f104-4117-ba60-174c5275e2fe

Yang, M., Bell, T. G., Hopkins, F. E., Kitidis, V., Cazenave, P. W., Nightingale, P. D., et al. (2016). Air-sea fluxes of CO_2 and CH_4 from the penlee point atmospheric observatory on the south-west coast of the UK. *Atmospheric Chemistry and Physics*, *16*(9), 5745–5761. https://doi.org/10.5194/acp-16-5745-2016

Yang, M., Prytherch, J., Kozlova, E., Yelland, M. J., Parenkat Mony, D., & Bell, T. G. (2016). Comparison of two closed-path cavity-based spectrometers for measuring air-water CO_2 and CH_4 fluxes by eddy covariance. *Atmospheric Measurement Techniques*, *9*(11), 5509–5522. https://doi.org/10.5194/amt-9-5509-2016

Ye, W., Arévalo-Martínez, D. L., Li, Y., Wen, J., He, H., Zhang, J., et al. (2023). Significant methane undersaturation during austral summer in the Ross Sea (Southern Ocean). *Limnology and Oceanography Letters*, *8*(2), 305–312. https://doi.org/10.1002/LOL2.10315

Yoshida, O., Inoue, H. Y., Watanabe, S., Suzuki, K., & Noriki, S. (2011). Dissolved methane distribution in the South Pacific and the Southern Ocean in austral summer. *Journal of Geophysical Research*, *116*(7), C07008. https://doi.org/10.1029/2009JC006089